Metal-rich fluid inclusions provide new insights into unconformity-related U deposits (Athabasca Basin and Basement, Canada).

Article:

Richard, A, Cathelineau, M, Boiron, MC et al. (3 more authors) (2016) Metal-rich fluid inclusions provide new insights into unconformity-related U deposits (Athabasca Basin and Basement, Canada). Mineralium Deposita, 51 (2). pp. 249-270. ISSN 0026-4598

https://doi.org/10.1007/s00126-015-0601-4

Mineralium Deposita

Metal-rich fluid inclusions provide new insights into unconformity-related U deposits (Athabasca Basin and Basement, Canada)

--Manuscript Draft--

Manuscript Number:	MIDE-D-14-00078R3
Full Title:	Metal-rich fluid inclusions provide new insights into unconformity-related U deposits (Athabasca Basin and Basement, Canada)
Article Type:	Regular Articles
Corresponding Author:	Antonin Richard FRANCE
Corresponding Author Secondary Information:	
Corresponding Author's Institution:	
Corresponding Author's Secondary Institution:	
First Author:	Antonin Richard
First Author Secondary Information:	
Order of Authors:	Antonin Richard
	Michel Cathelineau
	Marie-Christine Boiron
	Julien Mercadier
	David Banks
	Michel Cuney
Order of Authors Secondary Information:	
Funding Information:	
Abstract:	The Paleoproterozoic Athabasca Basin (Canada) hosts numerous giant unconformity-related uranium deposits. The scope of this study is to establish the pressure, temperature and composition (P-T-X conditions) of the brines that circulated at the base of the Athabasca Basin and in its crystalline basement before, during and after UO2 deposition. These brines are commonly sampled as fluid inclusions in quartz- and dolomite-cementing veins and breccias associated with alteration and U mineralization. Microthermometry and laser ablation - inductively coupled plasma - mass spectrometry (LA-ICP-MS) data from five deposits (Rabbit Lake, P-Patch, Eagle Point, Millennium and Shea Creek) complement previously published data for the McArthur River deposit. In all of the deposits investigated, fluid inclusion salinity is between 25 and 40 wt.% NaCl equiv., with compositions displaying a continuum between a "NaCl-rich brine" end-member (Cl>Na>Ca>Mg>K) and a "CaCl2-rich brine" end-member (Cl>Ca≈Mg>Na>K). The CaCl2-rich brine has the highest salinity and shows evidence for halite saturation at the time of trapping. The continuum of compositions between the NaCl-rich brine and the CaCl2-rich brine end-members combined with P-T reconstructions suggest anisothermal mixing of the two brines (NaCl-rich brine : 180 ± 30°C and 800 ± 400 bars; CaCl2-rich brine: 120 ± 30°C and 600 ± 300 bars) that occurred under fluctuating pressure conditions (hydrostatic to supra-hydrostatic). However because the two brines were U-bearing and therefore oxidized, brine mixing was probably not the driving force for UO2 deposition. Several scenarios are put forward to account for the Cl-Na-Ca-Mg-K composition of the brines, involving combinations of seawater evaporation, halite dissolution, mixing with a halite-dissolution brine, Mg/Ca exchange during dolomitization, Na/Ca exchange by albitization of plagioclase, Na/K exchange by albitization of K-feldspar and Mg-loss by Mg-rich alteration. Finally, the metal concentrations in the NaCl-rich and CaCl2-rich

	brines are among the highest recorded compared to present-day sedimentary formation waters or fluid inclusions from basin-hosted base metal deposits (up to 600 ppm U, 3000 ppm Mn, 4000 ppm Zn, 6000 ppm Cu, 8000 ppm Pb and 10000 ppm Fe). The $CaCl_2$-rich brine carries up to one order of magnitude more metal than the NaCl-rich brine. Though the exact origin of major cations and metals of the two brines remains uncertain, their contrasting compositions indicate that the two brines had distinct flow paths and fluid-rock interactions. Large-scale circulation of the brines in the Athabasca Basin and Basement was therefore a key parameter for metal mobility (including U) and formation unconformity-related U deposits.
Response to Reviewers:	Comments are included in the cover letter

Abstract

The Paleoproterozoic Athabasca Basin (Canada) hosts numerous giant unconformity-related uranium deposits. The scope of this study is to establish the pressure, temperature and composition (P-T-X conditions) of the brines that circulated at the base of the Athabasca Basin and in its crystalline basement before, during and after UO_2 deposition. These brines are commonly sampled as fluid inclusions in quartz- and dolomite-cementing veins and breccias associated with alteration and U mineralization. Microthermometry and laser ablation - inductively coupled plasma - mass spectrometry (LA-ICP-MS) data from five deposits (Rabbit Lake, P-Patch, Eagle Point, Millennium and Shea Creek) complement previously published data for the McArthur River deposit. In all of the deposits investigated, fluid inclusion salinity is between 25 and 40 wt.% NaCl equiv., with compositions displaying a continuum between a “NaCl-rich brine” end-member (Cl>Na>Ca>Mg>K) and a “$CaCl_2$-rich brine” end-member (Cl>Ca≈Mg>Na>K). The $CaCl_2$-rich brine has the highest salinity and shows evidence for halite saturation at the time of trapping. The continuum of compositions between the NaCl-rich brine and the $CaCl_2$-rich brine end-members combined with P-T reconstructions suggest anisothermal mixing of the two brines (NaCl-rich brine : 180 ± 30°C and 800 ± 400 bars; $CaCl_2$-rich brine: 120 ± 30°C and 600 ± 300 bars) that occurred under fluctuating pressure conditions (hydrostatic to supra-hydrostatic). However because the two brines were U-bearing and therefore oxidized, brine mixing was probably not the driving force for UO_2 deposition. Several scenarios are put forward to account for the Cl-Na-Ca-Mg-K composition of the brines, involving combinations of seawater evaporation, halite dissolution, mixing with a halite-dissolution brine, Mg/Ca exchange during dolomitization, Na/Ca exchange by albitization of plagioclase, Na/K exchange by albitization of K-feldspar and Mg-loss by Mg-rich alteration. Finally, the metal concentrations in the NaCl-rich and $CaCl_2$-rich brines are among the highest recorded compared to present-day sedimentary formation waters or fluid inclusions from basin-hosted base metal deposits (up to 600 ppm U, 3000 ppm Mn, 4000 ppm Zn, 6000 ppm Cu, 8000 ppm Pb and 10000 ppm Fe). The $CaCl_2$-rich brine carries up to one order of magnitude more metal than the NaCl-rich brine. Though the exact origin of major cations and metals of the two brines remains uncertain, their contrasting compositions indicate that the two brines had distinct flow paths and fluid-rock interactions. Large-scale circulation of the brines in the Athabasca Basin and Basement was therefore a key parameter for metal mobility (including U) and formation unconformity-related U deposits.

Keywords

Brines - Metals - Fluid inclusions - Unconformity - Uranium - Athabasca

Introduction

The Athabasca Basin hosts numerous high-grade “unconformity-related” U deposits, located close to the interface between the crystalline basement, the sedimentary cover and basement-rooted faults. Most of the current models for their formation involve basin-derived oxidizing brines that were enriched in U through fluid-rock interaction and deposited the UO_2 at or close to the unconformity. Some authors (e.g. Hoeve and Sibbald 1978; Wilson and Kyser 1987) also invoke a basement-derived reducing fluid as being responsible for U reduction during mixing with basin-derived brines (see Jefferson et al. 2007; and Kyser and Cuney 2008, for reviews of genetic models). Because basin-derived brines are thought to be the uranium carrier, reconstructing their pressure, temperature and composition (P-T-X conditions) is crucial for understanding the origin of the world’s richest U deposits. Bulk salinities, halogen (Cl–Br–I) and noble gas (Ar–Kr–Xe) systematics, and the stable chlorine isotopic composition of fluid inclusions as well as the boron isotopic composition of tourmaline, together indicate that these brines originated from sub-aerial evaporation of seawater (Derome et al. 2005; Richard et al. 2011; 2014; Leisen et al. 2012; Mercadier et al. 2012). Experimental work coupled with synchrotron-XRF, XANES and LA-ICP-MS analysis of fluid inclusions have shown that the U was probably transported in the form of uranyl(VI) chloride complexes, under low pH conditions and at the highest concentrations recorded for crustal fluids so far (pH = 2.5 to 4.5; [U] = 0.1 to ~ 600 ppm; Richard et al., 2010, 2012, 2013a; Dargent et al. 2013).

Many aspects of the Athabasca basin-derived brines remain controversial: (i) the origin of major solutes (i.e. seawater evaporation and/or fluid-rock interaction; Richard et al. 2010; Mercadier et al. 2012); (ii) the source of U and other metals (i.e. basin vs. basement rocks; Fayek and Kyser, 1997; Annesley and Madore 1999; Hecht and Cuney, 2000; Mercadier et al., 2013); and (iii) their P-T conditions (i.e. various estimates in the 80-300°C and 500-1500 bar ranges; Pagel

1975a, 1975b; Kotzer and Kyser 1995; Derome et al. 2005; Alexandre et al. 2005; Mercadier et al. 2010; Richard et al. 2013b).

In the Athabasca Basin, the only well-constrained deposit from a fluid inclusion perspective is the McArthur River deposit (Pagel and Ahamdach 1995; Kotzer and Kyser 1995; Derome et al. 2003, 2005; Richard et al. 2010, 2011, 2012, 2013a). Based on microthermometry, Raman spectroscopy and laser-induced breakdown spectroscopy (LIBS) analysis, Derome et al. (2005) concluded that a NaCl-rich brine had circulated at 220 ± 30°C and 1350 ± 150 bars, and a $CaCl_2$-rich brine had circulated at 110 ± 30°C and 700 ± 200 bars. Mixing between the two brines occurred during the pre-ore stage at 700 ± 200 bars after a pressure decrease from lithostatic to near hydrostatic conditions at 5-6 km depth. Using LA-ICP-MS analysis, detailed Na-Ca-Mg-K-Sr-Ba-U compositions of fluid inclusions were obtained that showed well-defined mixing trends between the NaCl-rich brine and the $CaCl_2$-rich brine end-members (Richard et al. 2010). In order to establish which characteristics of the McArthur River fluid inclusions could or could not be extrapolated to the entire Athabasca system, a microthermometric and LA-ICP-MS study of fluid inclusions was carried out on five deposits (Rabbit Lake, Shea Creek, Eagle Point, P-Patch and Millennium) located in various parts of the basin and above and below the unconformity.

Geology and sampling

Regional geology

The Athabasca Basin (Fig. 1a) unconformably overlies the Archean to Paleoproterozoic Western Churchill Province, which is separated into two subprovinces (the Rae Subprovince in the west and the Hearne Subprovince in the east) by the northeast-trending Snowbird tectonic zone (Hoffman 1990; Card et al. 2007; Jefferson et al. 2007). These two subprovinces consist of Archean gneisses, Paleoproterozoic metapelites and mafic to felsic intrusions and were affected by the ~2.0 to ~1.9 Ga Thelon-Talston and the ~1.9 to ~1.8 Ga Trans-Hudson orogenies, respectively (Chiarenzelli et al. 1998; Annesley et al. 2005). The majority of the known unconformity-related U deposits in the Athabasca Basin are located close to the transition between two lithostructural domains of the Hearne Subprovince, known as the Wollaston-Mudjatik transition zone (WMTZ), which consists of a northeast-trending, anastomosing structure of Hudsonian age (1.8 Ga) (Annesley et al. 2005).

The sedimentary sequence of the Athabasca Basin (the Athabasca Group) was deposited from about 1.75 Ga onwards (Ramaekers et al. 2007). The current maximum thickness of the sedimentary cover is ~1.5 km and could have reached around 5 km according to P-T estimates from fluid inclusions (Pagel, 1975a, 1975b; Derome et al. 2005). From the base to the top, the Athabasca Group is composed of fluvial to marginal marine quartz-rich sandstones (Fair Point, Read, Smart and Manitou Falls formations), marine sandstones, phosphatic siltstones and phosphatic mudstones (Lazenby Lake and Wolverine Point Formations), sandstones (Locker Lake and Otherside Formations), shales (Douglas formation) and finally stromatolitic carbonates (Carswell formation) (Ramaekers et al. 2007). The Douglas and Carswell formations are only preserved around the Carswell meteorite impact structure (Pagel et al. 1985; Genest et al. 2010).

Unconformity-related U deposits

The U deposits are generally located near the basement/cover interface and are structurally controlled by sub-vertical faults rooted in graphite-rich basement metapelites. The spatial distribution of the ore and alteration minerals around the unconformity varies greatly between the deposits. The UO_2 ores may be basement-hosted (e.g. P-Patch, Eagle Point and Millennium), unconformity-hosted (e.g. McArthur River, Rabbit Lake) or sandstone-hosted (e.g. Cigar Lake), sometimes within the same deposit (e.g. Shea Creek).

The earliest UO_2 ores in the Athabasca Basin have been dated to between 1.6 and 1.4 Ga and successive late episodes of recrystallization occurred until ~ 0.7 Ga (Cummings and Krstic 1992; Fayek et al. 2002; Alexandre et al. 2009; Alexandre et al. 2012). Remobilization of primary UO_2 by meteoric fluids along roll-fronts in basement rocks likely occurred from around 400 Ma and continued to recent times (Wilson et al. 1987; Kotzer and Kyser 1995; Mercadier et al. 2011a).

Alteration occurs on a large-scale in the Athabasca basin but is most extensively developed around the U-ores (Earle and Sopuck 1989; Quirt 2003). The main features include: (i) partial to complete replacement of the initial basement minerals (K-feldspar, biotite, plagioclase, hornblende) by an illite + sudoite (Mg-chlorite) ± dravite (Mg-tourmaline) assemblage (e.g. Alexandre et al. 2005; Mercadier et al. 2010), as well as the precipitation of quartz, illite and sudoite in the sandstone porosity (Kotzer and Kyser 1995; Lorilleux et al. 2002; Derome et al. 2005; Kister et al. 2006); (ii) quartz dissolution in basement rocks as well as in the sandstones (e.g. Lorilleux et al. 2003; Mercadier et al. 2010); (iii) precipitation of UO_2 in the alteration- and quartz dissolution-related porosity, as well as in veins and breccias (dravite + quartz ± dolomite ± bitumen also being found as cements in these mineralized or barren structures; e.g. Hoeve and Sibbald 1978; Derome et al. 2005); and (iv) rare earth element mobilization and redistribution among aluminium phosphate-sulphate minerals and UO_2 (e.g. Fayek and Kyser 1997; Gaboreau et al. 2007; Mercadier et al. 2011b).

Fluid inclusion nomenclature and previous studies

In this study, we use the fluid inclusion nomenclature defined by Derome et al. (2005) for the McArthur River deposit. Five fluid-inclusion types are defined on the basis of their microthermometric characteristics. Inclusions with a halite cube at room temperature are termed Lwh' or Lwh according to the last phase (ice or hydrohalite, respectively) to melt at low temperature and to the mode of homogenization (by halite or vapor disappearance, respectively) at high temperature. Inclusions that contained no halite cubes and whose last phase to melt at low temperature was hydrohalite, are noted Lw2. Inclusions that contained no halite cube and whose last phase to melt at low temperature was ice are noted Lw’ (-60°C < Tm ice < -30°C), Lw1 (-30°C < Tm ice < -15°C), or Lw’’ (-15°C < Tm ice < 0°C), where Tm ice is the temperature of ice-melting. Lw’ and Lwh’ inclusions frequently failed to nucleate ice during during cooling, even at temperatures as low as -190°C (about a third of these inclusions), preventing observation of first melting (Te) and ice melting (Tm ice). Previous LIBS and LA-ICP-MS analyses of McArthur River fluid inclusions have shown that Lw1, Lw2 and Lwh inclusions are more representative of the NaCl-rich brine, whereas Lw’ and Lwh’ are more representative of the $CaCl_2$-rich brine (Derome et al., 2005; Richard et al., 2010). Lw’’ inclusions were classified as late “low salinity fluids” by Derome et al. (2005) and are unrelated to NaCl-rich and $CaCl_2$-rich brines.

Previous fluid inclusion data for the McArthur River deposit are summarized in Table 1 (Derome et al. 2005; Richard et al. 2010) and show the contrasting compositions and microthermometric characteristics of fluid inclusions representative of the NaCl-rich brine (Lw1, Lw2, Lwh) and $CaCl_2$-rich brine (Lw’, Lwh’). Previous microthermometric data from the Athabasca Basin were compiled and fluid inclusions were tentatively classified according to the nomenclature used in this study (Table 2). Some fluid-inclusion types are widely represented across the previously studied areas (Lw1, Lwh, Lwh’’), while others are more scarce (Lw2, Lw’). This could be due to the difficulties in observing hydrohalite melting in Lw2 inclusions and to the fact that Lw’ inclusions frequently fail to nucleate ice upon cooling, which may have limited the reporting of microthermometric data for such fluid inclusions. However, this compilation does show that fluid inclusions representative of the NaCl-rich brine (Lw1, Lw2, Lwh) and $CaCl_2$-rich brine (Lw’, Lwh’) have been described in most of the deposits, as well as in unmineralized central parts of the basin (Rumpel Lake).

Quartz and dolomite and their fluid inclusions in the ore-forming process

It is generally agreed that quartz is spatially closely-associated with the main alteration minerals (illite, sudoite, dravite) and UO_2 (Dahlkamp 1978; Hoeve and Sibbald 1978; Wilson and Kyser 1987; Kotzer and Kyser 1995; Fayek and Kyser 1997; Kyser et al. 2000; Lorilleux et al. 2002; Derome et al. 2005; Kyser and Cuney 2008; Ng et al. 2013). Furthermore, carbonates (calcite, siderite and dolomite) are common in the Rabbit Lake, Shea Creek, Eagle Point and McArthur River deposits (Hoeve and Sibbald 1978; Pagel et al. 1980; Hoeve et al. 1986; Heine 1986; Lorilleux et al. 2002; Derome et al. 2005; Cloutier et al. 2011). Cross-cutting relationships suggest that quartz and dolomite (the only carbonate studied here) cannot be placed in a single position relative to UO_2 ore. For example, quartz has been variably interpreted as pre-ore (Ng et al. 2013), pre- to post-ore (Dahlkamp 1978; Hoeve and Sibbald 1978; Derome et al. 2005), syn-ore (Kotzer et al. 1992; Kotzer and Kyser 1995; Lorilleux et al. 2002) and post-ore (Alexandre et al. 2005; Cloutier et al. 2009). Dolomite mainly occurs in the basement and, when found in the same mineral assemblage, generally postdates associated quartz (Hoeve and Sibbald 1978; Derome et al. 2005). The relative timings of the growth of alteration minerals (illite, sudoite, dravite), quartz, dolomite and UO_2 can be difficult to ascertain because: (i) mineral deposition is often cyclic (Dahlkamp 1978; Hoeve and Sibbald 1978); (ii) the different stages are variably expressed in basement and sandstone lithologies (Kyser and Cuney 2008; Alexandre et al. 2009); and (iii) recurrent episodes of quartz dissolution may have occurred (Derome et al. 2005).

Consequently, it is always debatable as to whether a given sample contains fluid inclusions which are fully representative of the fluids involved at the main UO_2 stage. However, all fluid inclusion studies point to NaCl-rich and $CaCl_2$-rich brines as the uranium carrier and dominant fluid involved from the pre-ore, syn-ore to the post-ore stages: (i) sandstone silicifications, which is unanimously recognized as preceding the main UO_2 stage, show primary NaCl-rich and $CaCl_2$-rich brine inclusions at the Cluff Lake and McArthur River deposits (Table 2, Pagel 1975a, 1975b; Kotzer and Kyser 1995; Derome et al. 2005); (ii) the increasing intensity of illite-sudoite-dravite alteration is related to an increasing abundance of secondary NaCl-rich and $CaCl_2$-rich brine inclusion planes in magmatic and metamorphic quartz from basement rocks at the P-Patch deposit (Mercadier et al. 2010); (iii) pre- to post-ore quartz in barren and mineralized samples contain primary and pseudosecondary NaCl-rich and $CaCl_2$-rich brine inclusions (Pagel et al. 1980; Kotzer and Kyser 1995; Derome et al. 2005); (iv) the O isotopic composition of quartz shows that quartz-forming fluids (i.e. NaCl-rich and $CaCl_2$-rich brines) are isotopically equilibrated with illite, sudoite and dravite (Richard et al. 2013b); (v) halogen and noble gas systematics of NaCl-rich and $CaCl_2$-rich brine inclusions in quartz and dolomite and the B isotopic composition of dravite indicate a common evaporated seawater origin for the NaCl-rich and $CaCl_2$-rich brines and the dravite-forming fluids (Richard et al. 2011, 2014; Leisen et al. 2012; Mercadier et al. 2012); and (vi) LA-ICP-MS analysis of NaCl-rich and $CaCl_2$-rich brine inclusions in pre- to post-ore quartz and the inclusions were found to contain up to 600 ppm U (Richard et al. 2010, 2012) and Synchrotron-XRF and XANES analyses in NaCl-rich brine inclusions showed that the uranium was in the oxidized form, U(VI) (Richard et al. 2013a).

Sampling strategy

Because of the close association between the quartz, dolomite, alteration minerals and the UO_2, quartz and dolomite cements in veins and breccias were targeted as potentially hosting fluid inclusions that are representative of the dominant fluid involved at the time of alteration and mineralization.

Five uranium deposits from the Athabasca Basin were sampled for this study (Rabbit Lake, Shea Creek, P-Patch, Millennium and Eagle Point) and previously published data from the McArthur River deposit (P2 North orebody) were used for comparison (Derome et al. 2005; Richard et al. 2010), covering various mineralized areas in the basin (Fig. 1a). These deposits share the typical characteristics of unconformity-related U deposits described above.

Sampling focused on basement-hosted mineralization and alteration, largely because of a lack of preserved sedimentary cover (Rabbit Lake and Eagle Point) and lack of sandstone-hosted quartz and dolomite cements in veins or breccias (P-Patch and Millennium). Four samples that exhibited quartz cementing veins were selected in sandstones at Shea Creek (IF23, IF29, IF41, IF98), 20 to 30 m above the unconformity. For basement-hosted samples (33 quartz and 14 dolomite samples), the depth below the unconformity ranges from 13 m (EPE44-17, Eagle Point) to 361 m (EPE44-14, Eagle Point). A brief petrographic description of the samples is given in Electronic Supplementary Materials (ESM 1). Figure 2 illustrates some of the typical quartz and dolomite occurrences studied in this work.

The selected quartz and dolomite samples cement veins and breccias hosted by unaltered to strongly altered (illite-sudoite-dravite) rocks. Based on previous work on the McArthur River deposit only barren samples were selected for analysis: (i) water radiolysis around UO_2 ores can lead to enrichment in H_2 and O_2 causing abnormally high homogenization temperatures of fluid inclusions (Derome et al. 2003, 2005); (ii) mineralized samples can be problematic during LA-ICP-MS analysis because of the potential for surface contamination and the presence of U-rich quartz domains (Richard et al. 2010); and (iii) fluid inclusions with similar major and trace element contents have been found in both mineralized and barren samples (Derome et al. 2005; Richard et al. 2010).

Fluid inclusion petrography

Within the quartz and dolomite, the petrography of fluid inclusions is generally complex due to (i) alternating quartz growth and dissolution episodes; and (ii) intense microfracturing during mineral growth, leading to the formation of clusters of primary and pseudosecondary inclusions. Therefore, the application of the fluid inclusion assemblage concept (Goldstein and Reynolds 1994) is difficult in this context. These processes are recurrent throughout the formation of millimetre-sized quartz and dolomite, and primary and pseudosecondary inclusions could only be clearly distinguished from one another in rare cases (Fig. 2). Therefore, the inclusions analyzed are considered to be representative of a single fluid event associated with the filling of veins and breccias.

Two-phase (liquid-vapor) or three-phase (liquid-vapor-halite) fluid inclusions, 5 to 25 µm in size, are typically observed in both quartz and dolomite (Fig. 2). The volumetric proportion of the vapor phase is ~ 10%. Inclusions present negative crystal or more irregular shapes. A small number of inclusions contain solids with the presence of hematite and/or phyllosilicates, all interpreted to be daughter minerals due to their near constant volume relative to the volume of fluid inclusions.

Methods

Fluid inclusion microthermometry

Microthermometry was performed on fluid inclusions using a Linkam MDS600 heating-cooling stage. The temperatures of phase changes were measured for the following: first melting (Te), ice melting (Tm ice), hydrohalite melting (Tm hyd), halite dissolution (Ts NaCl) and homogenization to the liquid phase (Th). The temperatures of phase changes have a precision of about ± 5°C for Te, ± 0.1°C for Tm ice and Tm hyd, and ± 1°C for Ts NaCl and Th. The composition of fluid inclusions was calculated in the two-salt NaCl-$CaCl_2$-H_2O system or single-salt NaCl-H_2O and $CaCl_2$-H_2O systems, using microthermometric data and numerical models based on empirical best-fits of phase equilibria determined from experimental data. When only Tm ice was observed, fluid inclusion composition could only be calculated in single-salt systems NaCl-H_2O (Lw1 inclusions) or $CaCl_2$-H_2O (Lw´ inclusions) using the AqSo2 computer program (Bakker 2003). When at least two phase transitions were observed, the fluid inclusion composition was calculated in the NaCl-$CaCl_2$-H_2O system using Tm ice - Tm hyd pairs (Lw2 inclusions) or Tm ice - Ts NaCl pairs (Lwh and Lwh´ inclusions), using Steele-MacInnis et al. (2011). Isochores have been drawn on the basis of the mean salt content and the Th modes of the fluid inclusions using the FLUIDS 1 package (Bakker 2003) and the equations of Zhang and Frantz (1987).

LA-ICP-MS analysis of fluid inclusions

166 fluid inclusions from 9 quartz samples from the Rabbit Lake, P-Patch, Eagle Point and Millennium deposits, containing both NaCl-rich and $CaCl_2$-rich brine inclusions, were selected (ESM 1). LA-ICP-MS analysis of fluid inclusions was carried out at the School of Earth and Environment, University of Leeds, at instrumental conditions reported in Allan et al. (2005). Individual quartz-hosted fluid inclusions were ablated with a ArF 193 nm Geolas Q Plus excimer laser (Microlas, Göttingen, Germany). Ablation took place in an He atmosphere and the ablated material was transported by a 0.68-ml/min He flow to a mixing device where 1 $l.min^{-1}$ Ar was added. Ablated samples were subsequently analyzed in an Agilent 7500c Quadrupole ICP-MS equipped with an Octopole Reaction System. The analyses were run with the reaction cell pressurized with 2.5 $ml.min^{-1}$ H_2 in order to eliminate $^{40}Ar^+$ and $^{40}Ar^{16}O^+$ interferences on $^{40}Ca^+$ and $^{56}Fe^+$ and to reduce the high Ar-based backgrounds on $^{39}K^+$. The following elements were recorded: ^{7}Li, ^{23}Na, ^{24}Mg, ^{39}K, ^{40}Ca, ^{55}Mn, ^{56}Fe, ^{63}Cu, ^{66}Zn, ^{88}Sr, ^{137}Ba, ^{208}Pb and ^{238}U.

In all cases, ^{23}Na was used as internal reference element. Limits of detection (LODs) of the other elements were calculated using the 3σ criterion (Longerich et al. 1996). The analytical precision of most elements is within 15% RSD. For K, the analytical precision is better than 15% RSD. The analytical precision of the other elements is typically better than 30% RSD (Allan et al. 2005).

Calibration and signal-integration were performed with the Matlab®-based SILLS program (Guillong et al. 2008). Absolute element concentrations can be calculated from analyzed ratios relative to Na if this concentration is known. The Na concentration can be obtained from the salinity estimated from microthermometry (in wt.% NaCl equiv.) using the charge-balance technique (Allan et al. 2005). This method corrects the modelled amount of Na (from the wt.% NaCl equiv.) for contributions from other chloride salts using the analyzed elemental ratios to Na. Based on microthermometric measurements (ESM 2) a chlorinity of 6.5 molal was attributed to all inclusions, which should over- or underestimate absolute concentrations by a maximum of 30% relative, but more generally around 10% (Derome et al. 2005). Absolute element concentrations are given in ppm (equivalent $\mu g.g^{-1}$) and the complete LA-ICP-MS dataset is presented in ESM 3.

Results

Fluid inclusion distribution among samples

The absolute and relative abundances of the different microthermometric types of fluid inclusion in all samples are given in ESM 1. Microthermometric data and fluid inclusion compositions in the H_2O-NaCl-$CaCl_2$ system are summarized in ESM 2. Some samples contained only Lw1, Lw2 and Lwh, and others only Lw' and Lwh', however the majority of samples contained all types in variable proportions. Low salinity Lw'' inclusions were found very sporadically (ESM 2) and may represent relicts of late fluids, unrelated to the NaCl-rich and $CaCl_2$-rich brines (Derome et al. 2005). They are not discussed here. Quartz and dolomite have comparable fluid inclusion contents except for Lwh’ inclusions, which were almost only found in quartz (only one observation in dolomite). No relationship was found between fluid inclusion content, alteration and the depth relative to unconformity of the sample.

Fluid inclusion composition in the H_2O-NaCl-$CaCl_2$ system

The compositions of individual fluid inclusions are plotted in the ternary H_2O-NaCl-$CaCl_2$ diagram in Figure 3. Quartz and dolomite-hosted fluid inclusions cannot be distinguished. All deposits contain both Na-dominated and Ca-dominated inclusions as well as inclusions of intermediate composition. Taken together, the composition of fluid inclusions displays a continuum between NaCl-rich brine (20-25 wt.% salts) and a $CaCl_2$-rich brine (25-40 wt.% salts) end-member.

The Te of Lw1 inclusions is generally between -60 and -55°C, and Tm ice is between -30°C and -15°C with most observed values around -25°C (ESM 2). In the H_2O-NaCl-$CaCl_2$ system, Tm hyd can be higher or lower than Tm ice, and Tm ice - Tm hyd pairs are indicative of Na/Ca ratios. The case where Tm hyd is higher than Tm ice is typically represented by Lw2 inclusions (see below). Alternatively, if Tm hyd is lower than Tm ice, this would result in a wide range of possible Na/Ca ratios and possibly Ca-dominated compositions. In practice, the observation of hydrohalite melting before ice melting is complicated by the difficulty in distinguishing ice from hydrohalite when the two phases are mixed. Attempts to use sequential freezing to coarsen hydrohalite to observable sizes before ice melting (Haynes et al. 1985) were unsuccessful. Lw1 inclusions are therefore suspected to be metastable Lw2 inclusions that failed to nucleate any hydrohalite during cooling.

In Lw2 inclusions, Te is generally between -60 and -55°C and hydrohalite is the last phase to melt. Tm ice is centred on -25°C and Tm hyd between -21°C and +21°C (ESM 2). In the H_2O-NaCl-$CaCl_2$ system, hydrohalite melting is limited to the -21.0 to -0.1°C range. Here, positive Tm hyd indicates either stable hydrohalite melting in a more complex solution or metastable hydrohalite melting (Zwart and Touret 1994). Repeated measurements showed that Tm hyd were reproducible to within ± 1°C. Therefore, we consider positive Tm hyd to be the consequence of complex chemistry of the solutions. Although a wide range of molar Na/Ca ratios were calculated in Lw2 inclusions, most values centre on the 3-4 range.

Lwh inclusions generally have Te between -60 and -55°C. Tm ice is generally between -40 and -25°C and Tm hyd is observed in the majority of inclusions and is between -20 and +21°C (ESM 2). Ts NaCl is between 81 and 208°C. As for Lw2 inclusions, positive Tm hyd may indicate a complex chemistry of the solutions. Lwh inclusions have calculated Na/Ca ratios close to 5.

For about a third of Lw' inclusions, ice melting is not frequently observed due to the fact that fluid inclusions failed to nucleate ice during cooling, even at temperatures as low as -190°C. When ice formed, Te is between -70 and -60°C and Tm ice is between -55 and -30°C (ESM 2). These low Te and Tm ice values indicate a complex chemistry. As for Lw1 inclusions, hydrohalite melting theoretically occurs before ice melting. Attempts to use sequential freezing to coarsen hydrohalite to observable sizes before ice melting (Haynes et al. 1985) were unsuccessful. The field for possible compositions of Lw' inclusions in the H_2O-NaCl-$CaCl_2$ system is delimited by the H_2O-$CaCl_2$ axis and the hydrohalite field and ice melting isotherms (-55°C and -30°C; Fig. 3b) and results in Na/Ca ratios ranging from to 0.3 to near zero.

Lwh' inclusions exhibit low temperature behaviour comparable to Lw' inclusions and ice failed to nucleate during cooling even down to -190°C for about a third of these inclusions. Te is between -70 and -60°C and Tm ice is generally between -55 and -30°C. Ts NaCl is between 99 and 260°C. Calculated molar Na/Ca ratios mostly range from 0.3 to 1 (ESM 2).

Tm ice - Th pairs

Figures 4 and 5 show the Tm ice - Th pairs for quartz-hosted and dolomite-hosted fluid inclusions, respectively. The Th are highly variable and range from ~60°C to ~200°C for all fluid inclusion types. For both hosts, the Tm ice forms a continuum between ~ -15 and ~ -60°C. Th is highly variable (± 70°C) for every restricted range of Tm ice. For quartz-hosted inclusions, all deposits show a majority of Tm ice values scattered around -25°C and less frequent Tm ice data below -30°C. Note that for the later inclusions (Lw' and Lwh') Tm ice could not be systematically reported. This might explain some of the gaps in the continuum between the lowest Tm ice data (~-55°C) and the highest Tm ice values (~25°C) where fewer data could be acquired (P-Patch, Millennium). For quartz-hosted inclusions, the majority of observed Tm ice - Th pairs indicate a general decrease in Th with Tm ice (Fig. 4), with the two end-members being the NaCl-rich brine (Tm ice = ~ -20 to -30°C and most Th values between 100 and 150°C) and the $CaCl_2$-rich brine (Tm ice = ~ -50 to -60°C and most Th values of between 80 and 130°C). The only exception is the NaCl-rich brine inclusions at McArthur River, which have a significantly the higher Th distribution (most Th values between 120 and 170°C). A comparable trend of a general decrease in Th with Tm ice could approximately fit the dolomite-hosted inclusion data (Fig. 5).

Ts NaCl - Th pairs

Figure 6a shows Ts NaCl - Th pairs for quartz and dolomite-hosted Lwh and Lwh' inclusions. Most Lwh inclusions scatter close to the 1:1 slope whereas the majority of Lwh' inclusions scatter to the right of the 1:1 slope. The temperature difference between Ts NaCl and Th is represented as Δ(Ts NaCl - Th) and shows a continuum between -107°C and 216°C (Fig. 6b). While the volumetric proportion of vapor phase is always close to 10% of the total fluid inclusion volume, the volume of the NaCl phase shows the highest variability (up to twice the volume of the vapor phase). Consequently, the Lwh and Lwh' inclusions have been classified as a function of the volumetric relationship between NaCl and the vapor phase, into three groups: inclusions in which the volume of the NaCl phase (V(NaCl)) is lower, equal or higher than the volume of the vapor phase (V(vap)). Figure 6b shows that the highest Δ(Ts NaCl - Th) values are associated with fluid inclusions where V(NaCl) > V(Vap), and conversely, the lowest Δ(Ts NaCl - Th) values are associated with fluid inclusions where V(NaCl) < V(Vap).

Fluid inclusion compositions analyzed by LA-ICP-MS

A continuum of fluid inclusion compositions is observed between a low-Na end-member and a high-Ca end-member (Fig. 7, ESM 3). This dataset cannot be fully representative of all the possible compositions in each deposit due to the relatively small number of samples investigated (e.g. the absence of Ca-rich compositions at Eagle Point). At the sample scale, although neither microthermometry nor LA-ICP-MS analysis can be considered fully representative of the overall fluid inclusion variability due to the relatively small number of inclusions analyzed, the distribution of Na-dominated inclusions and Ca-dominated inclusions are consistent with the distribution seen in microthermometry data (Fig. 3, 7; ESM 1, 3). While there may be some minor differences between deposits, the continuum was observed in most localities. The LA-ICP-MS data will therefore be described and discussed for all deposits together.

The proportions of fluid inclusions with element concentrations above the LOD are as follows: Li (85%); Na (100%); Mg (100%); K (93%); Ca (100%); Mn (52%); Fe (94%); Cu (42%); Zn (70%); Sr (99%); Ba (86%); Pb (82%) and U (63%). In inclusions in which the elements could be quantified, the absolute content of every analyzed element is highly variable: Li = 40 to 16000 ppm; Na = 5400 to 140000 ppm; Mg = 590 to 53000 ppm; K = 930 to 52000 ppm; Ca = 640 to

96000 ppm; Mn = 38 to 2800 ppm; Fe = 32 to 16000 ppm; Cu = 2 to 6300 ppm; Zn = 6 to 4400; Sr = 9 to 2800 ppm; Ba = 11 to 2100 ppm; Pb = 3 to 8100 ppm and U = 0.2 to 610 ppm (ESM 3).

Assuming that the high Na concentrations relate to the NaCl-rich brine and the low Na concentrations relate to the $CaCl_2$-rich brine, it is possible to identify the likely composition range for the NaCl-rich brine and $CaCl_2$-rich brine end-members. If Na concentrations of >80000 ppm and <30000 ppm are representative of the NaCl-rich brine and $CaCl_2$-rich brine end-members, respectively (Richard et al. 2010), the distributions of cation concentrations in each end-members can be approached (Fig. 8). The $CaCl_2$-rich brine shows significant enrichment (up to one order of magnitude) in Mg, K, Ca, Fe, Cu, Zn, Sr, Ba, Pb and U compared to the NaCl-rich brine (Fig. 8). The NaCl-rich brine is characterized by Cl>Na>Ca>Mg>K brine whereas the $CaCl_2$-rich brine is a Cl>Ca≈Mg>Na>K brine (Fig. 8). U concentration data have already been published and discussed in detail in Richard et al. (2012).

Discussion

P-T-X conditions and scales for brine circulations

According to Ts NaCl - Th relationships and volumetric considerations on vapor and NaCl phases (Fig. 6), the $CaCl_2$-rich brine was probably saturated with respect to halite at the time of trapping (Becker et al. 2008). In this case, NaCl cubes would have been trapped heterogeneously along quartz growth planes and fluid inclusions. During cooling to (sub)surface conditions after trapping, the halite would either have nucleated within halite-free inclusions or coarsened from the previously trapped NaCl nuclei. Given such a scenario, it is therefore possible that the Na concentration in the $CaCl_2$-rich brine has been overestimated. Indeed, if NaCl crystals precipitated in the hydrothermal solutions and were heterogeneously trapped within fluid inclusions mechanically, then the compositions of the fluid inclusions may be richer in NaCl than the actual composition of the brine. The causes of NaCl saturation at the time of trapping are uncertain. NaCl-saturation can originate from (i) cooling of a high-temperature and high-salinity brine; (ii) salt enrichment by H_2O uptake from brines to alteration minerals (Gleeson et al. 2003); or (iii) leaching of Cl from Cl-bearing minerals. The first hypothesis cannot be completely excluded, however this would imply trapping temperatures in excess of 250°C, which is above temperature estimates from mineral thermometers in this context (Alexandre et al. 2005). The second and third hypotheses are supported by the increase in the salinity of fluid inclusions, where alteration is most intense (Mercadier et al. 2010), and the ~ 90% loss of Cl in altered rocks compared to their fresh counterparts as a result of biotite breakdown (Richard et al. 2011). The influence of the last two phenomena relies on the fluid-rock ratios, which to date remain poorly constrained.

The observed scatter of Th values observed in the Tm ice vs Th diagrams (Fig. 4) might be explained by: (i) post-trapping reequilibration; (ii) partial leakage during heating; (iii) pressure fluctuations during trapping; or (iv) heterogeneous contamination by trace gases. Post-trapping reequilibration is commonly observed in diagenetic minerals (Goldstein 2001; Bodnar 2003). Such modifications lead to changes in fluid inclusion density and variation of the volumetric fraction of the vapor phase. Variation of the volumetric fraction of vapor phase within the range of the present observations (< 10% relative) could lead to significant Th variation (several tens of degrees; Bodnar 2003). The 50-100°C variation in Th observed within some quartz-hosted and dolomite-hosted fluid inclusion clusters supports this hypothesis. However, there is no clear optical evidence for post-trapping re-equilibration. Partial leakage during heating frequently occurs in diagenetic minerals, especially in carbonate cements (Goldstein and Reynolds 1994). It could well be that some of the highest Th measured in dolomite have been affected by partial leakage, however there is no clear optical evidence for this here. Pressure fluctuations between hydrostatic (lower limit) and supra-hydrostatic regimes (upper limit) could account for around 40°C of Th variation if pressure varies between purely hydrostatic and purely lithostatic (Dubessy et al. 2003). Pressure fluctuations in the brines are predicted by seismic pumping (Behr et al. 1987). Over-pressuring (i.e. supra-hydrostatic pressure) is also a common phenomenon in burial diagenesis (Swarbrick and Osborne 1997) although a hydrostatic pressure regime appears to be the rule rather than the exception in the Athabasca Basin (Cui et al. 2012a, 2012b; Chi et al. 2013). Contamination of fluid inclusions by trace gases, even if not optically visible, is likely to lead to anomalously high Th. This hypothesis has already been proposed for high Th values measured in the rare secondary low-salinity fluid inclusions at McArthur River (Derome et al. 2005) and the detection of trace amounts of CO_2, CH_4, H_2 and O_2 in brine inclusions by Raman spectroscopy was shown in Derome et al. (2003). Here, we propose that gas contamination may have affected the two brines, possibly leading to the highest measured Th (> 150°C).

On the basis of these assumptions, a reconstruction of P-T conditions for NaCl-rich and $CaCl_2$-rich brines in unconformity-related deposits can be attempted. Isochores were drawn from the most likely representative Th range for the two brine end-members in both quartz and dolomite: 80-130°C for the $CaCl_2$-rich brine and 100-150°C for the NaCl-rich brine (Fig. 9). Ts NaCl for Lwh' inclusions were not taken into account because the $CaCl_2$-rich brine was saturated with respect to halite at the time of trapping and only Th should represent the minimum trapping temperature (Becker et al. 2008). The slopes of the isochores are slightly steeper for $CaCl_2$-rich brines than for NaCl-rich brine inclusions due to their higher salinity. The P-T domain for trapping is constrained by the isochores, the hydrostatic thermal gradient (lower limit) and the lithostatic thermal gradient (upper limit). Note that in this model, static and reasonably low geothermal gradients (30-40°C / km) are assumed, which is not always the case in fluid systems that show rapid downflow or upflow as was possibly the case here (Bons et al. 2014). Therefore, such P-T reconstruction should be considered with caution. From this, it can reasonably be deduced that the $CaCl_2$-rich brine was trapped at 120 ± 30°C and 600 ± 300 bars and the NaCl-rich brine at 180 ±

30°C and 800 ± 400 bars (Fig. 9). Given that the depth below unconformity for the samples studied is negligible compared to the thickness of the basin, the calculated past thickness of the Athabasca Basin was ~ 3-6 km (Fig. 9). This P-T reconstruction is compatible with that of Derome et al. (2005) based on McArthur River fluid inclusions. Our temperature estimate for the NaCl-rich brine (180 ± 30°C) is compatible with independent thermometers based on illite and chlorite chemistry and the oxygen isotope composition of quartz-tourmaline pairs, which generally give temperatures of around 200°C (Kotzer and Kyser 1995; Ng et al. 2013). The estimated temperature of the $CaCl_2$-rich brine (120 ± 30°C) however, differs significantly from that derived from the independent thermometers. This could imply that the low temperature $CaCl_2$-rich brine was not recorded by the independent geothermometers, i.e., it was not involved to any great extent in the alteration of illite-sudoite-dravite. However, this does not mean that the low-temperature event was a late event. For example, Derome et al. (2005) demonstrated that the low-temperature $CaCl_2$-rich brine was responsible for pervasive sandstone silicification prior to the UO_2 stage and that higher temperature NaCl-rich brine was also present before and after the UO_2 stage. The temperature difference between the NaCl-rich and $CaCl_2$-rich brine might be explained by physical separation of the two reservoirs. Derome et al. (2005) tentatively suggested that the cooler $CaCl_2$-rich brine originated from the upper levels of the Athabasca Basin and percolated into the basement rocks without any significant temperature re-equilibration, acquiring its Ca-rich composition before reaching deposit sites. Although the occurrence of NaCl-rich brines and cooler $CaCl_2$-rich brines both originating from seawater evaporation appears to be usual in Proterozoic basins (Boiron et al. 2010), this temperature difference is far from fully understood and points out the need for further hydrogeochemical modelling (Raffensperger and Garven 1995; Cui et al. 2012a, 2012b).

Finally, the overall continuity of microthermometric data and detailed compositions between the NaCl-rich brine and the $CaCl_2$-rich brine end-members (Figs. 4, 5, 7) suggests that the data that plot between the two end-members represent mixing terms. Moreover, the overall trend of a slight decrease in Th from the NaCl-rich brine to the $CaCl_2$-rich brine end-members, as well as the P-T reconstruction (Fig. 9), are in favor of anisothermal mixing between the two brines. Causes of mixing of two physically-separated brine reservoirs could include the reactivation of basement-rooted faults controlling alteration and mineralization on both sides of the unconformity and the associated dense network of microfractures in basement rocks (Mercadier et al. 2010). Seismic pumping could have driven brines from different reservoirs towards these fault zones (Behr et al. 1987). Although brine mixing was systematically associated with alteration and UO_2 deposition, mixing itself could not have been the cause of reduction of U(VI) to U(IV) and subsequent UO_2 deposition because both brines were U-bearing and were therefore oxidized.

The new data from this study, in combination with the previously published data (Table 2), together suggest that the basal sandstones of the Athabasca Group as well as the upper part of the Athabasca Basement can be considered as a giant brine aquifer, at least at the scale of the present-day Athabasca Basin. Knowledge of the vertical extent of brine circulation in the basement is hindered by the lack of deep drill holes. The deepest known UO_2 mineralization in the basement (400 m below the unconformity at Eagle Point) indicates a minimal depth for brine percolation. The present-day maximum thickness of the basin is 1.5 km at Rumpel Lake. Assuming a past thickness of around 3 to 6 km and a relatively flat-lying basement, the past extent of the basin could have been much greater. As some deposits described in this study are located close to the basin margins (Rabbit Lake) and even outside of the basin margins (Eagle Point), it can be inferred that the circulation of the NaCl-rich and $CaCl_2$-rich brines extended beyond the present-day limits of the basin, and that unconformity-related deposits are likely to have formed away from the present-day limits. Interestingly, Mercadier et al. (2013) described alteration features typical of unconformity-related U deposits around 20 km east of the present-day Athabasca Basin margins.

Origin and behavior of major solutes and metals

Many factors control the salinity and chemistry of basinal brines, including the composition of seawater, evaporation of seawater, evaporite dissolution, dilution by meteoric water and/or seawater, mixing of waters with different chemistry, and mineral buffering (Hanor 1994; Davisson and Criss 1996; Houston et al. 2011). A common origin for the NaCl-rich and $CaCl_2$-rich brine end-members identified in this study has been demonstrated from analysis of halogen (Cl–Br–I) and noble gas (Ar–Kr–Xe) systematics and stable chlorine isotopic compositions of fluid inclusions (Derome et al. 2005; Richard et al. 2011, 2014; Leisen et al. 2012). The halogen data show that the two brines originated from a "parent brine" resulting from evaporation of seawater up to epsomite saturation, leading to their high salinity. The composition of seawater at the time of sedimentation in the Athabasca Basin remains unknown. The chemistry of evaporated seawaters is strongly dependent on the initial seawater composition, which is thought to have oscillated throughout the Phanerozoic and Neoproterozoic, between modern-like "$MgSO_4$ seas" and Cretaceous-like "$CaCl_2$ seas" (Lowenstein et al. 2001; Kovalevych et al. 2006). Whether the composition of seawater was modern- or Cretaceous-like during sedimentation in the Athabasca Basin is unknown and both hypotheses will be considered here. Evaporated seawater derived from "$CaCl_2$ seas" is considerably more Ca-rich (although Na-dominated) than that derived from "$MgSO_4$ seas" (Lowenstein et al. 2001; Lowenstein and Timofeeff 2008). The compositions of the NaCl-rich and $CaCl_2$-rich brine end-members do not plot between the epsomite-saturated evaporated seawater compositions for "$MgSO_4$ seas" and "$CaCl_2$ seas", which may represent two extremes (Fig. 7). Regardless of the seawater chemistry, it is clear that both NaCl-rich and $CaCl_2$-rich brines have compositions distinct from that of their "parent brine". Therefore, it appears that the compositions of the two brines are controlled not only by seawater evaporation, but also by different types of fluid-rock or fluid-fluid interactions. As the salinity of the NaCl and $CaCl_2$-rich brines is close to that of epsomite-saturated evaporated seawater, it is assumed that most of the reactions that significantly contributed to the modification of the composition of the initial evaporated seawater are ion exchange reactions or mixing between brines of comparable salinity. In Figure 7, the directions of compositional shifts expected for some typical fluid-rock or fluid-fluid interactions have been plotted. The interactions considered are: (1) halite dissolution or mixing with halite-dissolution fluid, which leads to Na-dominated compositions; (2) dolomitization of calcite (1:1 Mg/Ca exchange); (3) albitization of plagioclase (2:1 Na/Ca exchange); (iv) albitization of K-feldspar (1:1 Na/K exchange) and (5) Mg-alteration typical of unconformity-related U deposits (replacement of initial silicates, except quartz, by sudoite and dravite). Mg alteration is broadly characterized by Mg input and Ca-Na-K loss in the altered rocks. The precise chemical budget of Mg-alteration is difficult to constrain, the relative and absolute amounts of Ca, Na and K lost being dependent on the lithology and degree of alteration (Alexandre et al. 2005). In Figure 7, Mg-alteration is represented as net Mg-loss in the fluid. If the composition of the parent brine was that of "$MgSO_4$ seas" evaporated-seawater, then the composition of the NaCl-rich brine is best explained by a combination of halite dissolution or mixing with halite-dissolution fluid, Mg-alteration, dolomitization and albitization. In the same scenario, the composition of the $CaCl_2$-rich brine is best explained by a combination of albitization and dolomitization. If the composition of the parent brine is that of a "$CaCl_2$ seas" evaporated-seawater, then the composition of the NaCl-rich brine is best explained by halite dissolution or mixing with halite-dissolution fluid alone. In the same scenario, the composition of the $CaCl_2$-rich brine can be explained by albitization alone. Dolomitization and mixing with halite-dissolution brine (or halite dissolution) can occur at shallow depths, close to the depositional environment. Note that mixing with halite-dissolution brine is preferred to halite dissolution because the investigated brines are highly saline and would probably not have been able to dissolve halite. Albitization could have occurred at greater depth in the basin (in the eroded part because no detrital K-feldspars/plagioclase are currently present) or in the basement. Petrographic evidence for albitization due to basinal brines in the basement is lacking. However, sampling has been limited to relatively shallow drillcores and albitization at depth in the basement cannot be ruled out. The influence of Mg-alteration is difficult to ascertain. Though Mg-alteration could explain part of the variability in the Mg concentration of the $CaCl_2$-rich brine end-member and part of the Mg-depleted composition of the NaCl-rich brine end-member, it is not the dominant control on the brine chemistry. Taken together, the fluid inclusion data are most simply explained by considering a "$CaCl_2$ seas" evaporated-seawater parent brine. In order to form the $CaCl_2$-rich brine, the parent brine may have escaped dolomitization and mixing with halite-dissolution brine, probably by migrating from the evaporitic environment (laterally and/or vertically) shortly after the evaporative process, and then undergone albitization. In order to form the NaCl-rich brine, the parent brine is more likely to have remained spatially connected to the evaporitic environment and was more susceptible to modification by halite dissolution and/or mixing with halite-dissolution brine and dolomitization (Warren 1997; Houston et al. 2011). It is clear that these assumptions are only a first-order approach to the fluid-rock interactions that could have occurred in the Athabasca Basin. For example, the importance of mixing with halite-dissolution brines has probably been overestimated because the large contribution of halite-dissolution brine to the composition of the NaCl-rich brine cannot account for the observed Cl/Br ratios and δ^{37}Cl values of fluid inclusions (Richard et al. 2011; 2014; Leisen et al. 2012). Moreover, estimating the contributions of each of the reactions invoked is complicated by the number of reactions considered and the uncertainties in the compositions of parent brines and brine end-members. Nevertheless, the two brines may have had very distinct interaction histories and consequently, distinct pathways.

Metal-rich basinal brines are commonly sampled from boreholes or fluid inclusions and the connection between basinal brines and basin-hosted mineral deposits has been established in several studies (Carpenter et al. 1974; Sverjensky 1984, 1989; Kharaka et al. 1987; Kharaka and Hanor 2003; Wilkinson et al. 2009; Richard et al. 2012). The metal concentrations in the Athabasca brines can be compared with those of present-day sedimentary formation brines and those derived from LA-ICP-MS analysis of fluid inclusions from various basin-hosted base-metal ore deposits worldwide (Fig. 10). This comparison is limited by the limits of detection for metals by LA-ICP-MS which precludes the determination of metals with concentrations below 0.1 ppm. The Athabasca brines have Ba, Mn, Zn and Pb concentrations comparable to the highest concentrations recorded in sedimentary formation brines, whereas Fe, Cu and, more spectacularly, U concentrations are clearly above the richest Fe, Cu and U-bearing sedimentary formation brines (Carpenter et al. 1974; Kraemer and Kharaka 1986; Kharaka et al. 1987; Banner et al. 1990; Connolly et al. 1990; Stueber and Walter 1991; Land and Macpherson 1992; Pluta and Zuber 1995; Hodge et al. 1996; Hitchon et al. 2001; Aquilina et al. 2002). The Athabasca brines have Fe, Ba, Mn, Cu, Zn, Pb concentrations that are comparable to the highest concentrations recorded by LA-ICP-MS analysis of fluid inclusions in basin-hosted base metal ore fluids (Appold et al. 2004; Stoffell et al. 2004; Bouch et al. 2006; Huizenga et al. 2006; Piqué et al. 2008; Stoffell et al. 2008; Sanchez et al. 2009; Wilkinson et al. 2009; Appold and Wenz, 2011). No data is available for U concentrations in basin-hosted base metal ore fluids. The U concentrations in the Athabasca brines are among the most elevated concentrations recorded for geological fluids so far and are discussed in detail in Richard et al. (2012). However, other U deposits also show ore-forming brines with U concentrations of tens of ppm (Eglinger et al. 2014; Hurtig et al. 2014) meaning this could be a more general characteristic of U ore-forming fluids. Basinal brines can be driven through basement rocks in response to basement fracturing, resulting in intense fluid-rock interaction and metal extraction, and ultimately in the formation of Pb, Zn, Cu, F, Ba and U deposits close to the basement-cover interface (e.g. Shelton et al. 1995; Gleeson et al. 2000; Boiron et al. 2002, 2010; Feltrin et al. 2003; Kendrick et al. 2005; Wilkinson et al. 2005; Muchez et al. 2005; McGowan et al. 2006; Oliver et al. 2006; Kozyi et al. 2009; Mercadier et al. 2010; Cathelineau et al. 2012; Fusswinkel et al. 2014). Petrological and geochemical evidence for U mobilization from the

Athabasca Basement sources (e.g. monazite, pre-Athabasca Basin UO_2) is widespread (Annesley and Madore 1999; Hecht and Cuney 2000; Cuney et al. 2010; Mercadier et al. 2013). If, as indicated by the contrasting metal loads of the two brine end-members (Fig. 8), the $CaCl_2$-rich brine acquired more metals than the NaCl-rich brine and if the basement is effectively the main U source, then it could well be that the $CaCl_2$-rich brine leached metals from the basement more efficiently than the NaCl-rich brine.

Hacini and Oelkers (2011) have shown that U can be conservative during evaporative processes. This means that no U-bearing phase precipitates and the U is not substituted by any other elements in the evaporitic minerals during evaporation. Li is another conservative element during evaporation. Therefore, Li/U ratios should remain constant during seawater evaporation. Assuming Li and U concentrations in seawater of 170 and 3.3 ppb, respectively (Ku et al. 1977; Drever 1982) and a Li concentration in epsomite-saturated evaporated seawater of ~10 ppm (Fontes and Matray 1993), the U concentration in epsomite-saturated evaporated seawater should be close to 0.2 ppm. This corresponds to the lowest U concentration measured during LA-ICP-MS analysis of fluid inclusions. Hence, it is possible that evaporation of seawater was the first U-enrichment process to occur in the studied brines, although further strong enrichment is required to account for the high U concentrations in the fluid inclusions. Given the solubility of U(VI) in such brines, and the U concentrations measured in the fluid inclusions, the pH of the NaCl and $CaCl_2$-rich brines may have been between 2.5 and 4.5 (Richard et al. 2012). The acidic nature of the brines may also have promoted the transport of Ba, Mn, Cu, Pb, and Zn. The redox processes at the origin of UO_2 deposition are still poorly understood (Hoeve and Quirt 1987; Richard et al. 2013a) and will not be discussed here, but they were probably active only at the ore deposit sites as similar NaCl- and $CaCl_2$-rich brines were present not only in mineralized but also in unmineralized areas such as Rumpel Lake (Table 2). Although the Athabasca brines have metal concentrations comparable to those of a number of world-class basin-hosted base metal deposits (Fig. 10), the absence of deposition of Pb, Zn, Ba or Cu-bearing sulphide phases is intriguing. Minor sulphide and arsenide minerals containing Fe, Ni, Co, Cu, Pb, Zn, As, Mo and occasionally Au, Ag, Se and platinum group elements, have been identified around the studied deposits (Ruzicka 1989). However, the precise paragenetic position of these minerals with respect to U deposition remains unclear. The only significant S-bearing alteration minerals found here are the aluminium phosphate-sulphate minerals (Gaboreau et al. 2007). In general, causes for deposition of base metal sulphides in basinal settings are (i) reduction of sulfate to reduced sulfur by thermochemical sulfate reduction (TSR) or bacterial sulfate reduction (BSR) (Machel 2001); and (ii) mixing between metal-bearing fluids with cooler and/or dilute fluids which favors destabilization of metal complexes or with H_2S-bearing fluids. The Athabasca brines contain negligible sulfates (Richard et al. 2011) and Raman investigation of fluid inclusions revealed an absence of H_2S (Derome et al. 2003). Furthermore, the Athabasca brines did not mix with low-salinity-fluids. Therefore, the conditions for base metal deposition were not met in the Athabasca system.

Conclusion

Microthermometry and LA-ICP-MS analysis of fluid inclusions from five unconformity-related U deposits in the Athabasca Basin and Basement (Canada) allows to define the general characteristics of the metal-rich brines that were the dominant fluids involved before, during and after UO_2 deposition:

(1) NaCl-rich and $CaCl_2$-rich brines previously described at the McArthur River deposit have been reported for all of the newly studied deposits (Rabbit Lake, P-Patch, Eagle Point, Shea Creek and Millennium). A reappraisal of previously published fluid inclusion data suggest that these brines were also present in all previously studied deposits (Midwest, Cluff Lake,

Sue C - McClean, Key Lake), and also in unmineralized central parts of the basin (Rumpel Lake). Brine circulation was therefore probably basin-scale.

(2) The NaCl-rich brine (T-P: 180 ± 30°C and 800 ± 400 bars) and the $CaCl_2$-rich brine (T-P: 120 ± 30°C and 600 ± 300 bars) have mixed in all deposits, under pressure conditions that have probably fluctuated between hydrostatic and supra-hydrostatic. However, the two brines show U contents indicative of relatively high oxygen fugacity. Therefore, brine mixing was probably not the driving force for uranium reduction and precipitation.

(3) The two brines were chemically differentiated from their common parent composition (epsomite-saturated evaporated seawater) along distinct flow paths and fluid-rock interaction. The NaCl-rich brine underwent a possible combination of Mg/Ca exchange by dolomitization, mixing with halite-dissolution brine and Na/Ca and/or Na/K exchange by albitization. The $CaCl_2$-rich brine underwent nearly complete Na/Ca and/or Na/K exchange possibly by albitization.

(4) The two brines have high metal contents, the $CaCl_2$-rich brine being up to one order of magnitude more enriched in Cu, Pb, Zn, Mn and U. The metal concentrations are higher than in high-salinity sedimentary formation waters worldwide and are comparable to those found in fluid inclusions from basin-hosted Pb-Zn deposits, for which a basement metal source has been frequently invoked.

Finally, this study shows that the most spectacular uranium province in the world resulted from large-scale circulation of surface-derived brines (evaporated seawater), over hundreds of kilometres laterally, across an entire 3-6 km-thick sedimentary pile and at least several hundreds of meters below the unconformity in the crystalline basement. Such a large-scale brine circulation may have been a key parameter for the mobilization of huge amounts of uranium and other metals in the mineralizing systems.

Acknowledgements

The authors thank CNRS and Areva NC for the financial support (BDI CNRS-Areva NC PhD grant for A. Richard and J. Mercadier); Donatienne Derome for early microthermometric work; Areva NC and Cameco for providing the samples and Cédric Demeurie for preparation of doublypolished thick sections. The authors greatly appreciated insightful comments by Guoxiang Chi on an earlier version of this paper. The comments of two anonymous reviewers as well as the editorial suggestions from Rolf Romer and Georges Beaudoin helped to greatly improve the manuscript.

References

Alexandre P, Kyser K, Polito P, Thomas D (2005) Alteration mineralogy and stable isotope geochemistry of Paleoproterozoic basement-hosted unconformity-type uranium deposits in the Athabasca Basin, Canada. Econ Geol 100:1547–1563

Alexandre P, Kyser K, Thomas D, Polito P, Marlat J (2009) Geochronology of unconformity-related uranium deposits in the Athabasca Basin, Saskatchewan, Canada and their integration in the evolution of the basin. Miner Deposita 44:41–59

Alexandre P. Kyser K, Jiricka D, Witt G (2012) Formation and evolution of the Centennial unconformity-related uranium deposit in the South-Central Athabasca Basin, Canada. Econ Geol 107:385–400

Allan MM, Yardley BWD, Forbes LJ, Shmulovich KI, Banks DA, Shepherd TJ (2005) Validation of LA-ICP-MS fluid inclusion analysis with synthetic fluid inclusions. Am Mineral 90:1767–1775

Annesley IR, Madore C (1999) Leucogranites and pegmatites of the sub-Athabasca basement, Saskatchewan: U protore? In: Stanley CJ et al. (eds.), Mineral Deposits: Processes to Processing. Balkema, Rotterdam, pp 297–300

Annesley IR, Madore C, Portella P (2005) Geology and thermotectonic evolution of the western margin of the Trans-Hudson Orogen: Evidence from the eastern sub-Athabasca basement, Saskatchewan. Can J Earth Sci 42:573–597

Appold MS, Numelin TJ, Shepherd TJ, Chenery SR (2004) Limits on the metal content of fluid inclusions in gangue minerals from the Viburnum Trend, Southeast Missouri, determined by laser ablation ICP-MS. Econ Geol 99:185–198

Appold MS, Wenz ZJ (2011) Composition of ore fluid inclusions from the Viburnum Trend, Southeast Missouri district, United States: Implications for transport and precipitation mechanisms. Econ Geol 106:55–78

Aquilina L, Ladouche B, Doerfliger N, Seidel JL, Bakalowicz M, Dupuy C, Le Strat P (2002) Origin, evolution and residence time of saline thermal fluids (Balaruc springs, southern France): implications for fluid transfer across the continental shelf. Chem Geol 192:1–21

Bakker RL (2003) Package FLUIDS 1. Computer programs for analysis of fluid inclusion data and for modelling bulk fluid properties. Chem Geol 194:3–23

Banner JL, Wasserburg GJ, Chen JH, Moore CH (1990) ^{234}U-^{238}U-^{230}Th-^{232}Th systematics in saline groundwaters from central Missouri. Earth Planet Sci Lett 101:296–312

Becker SP, Fall A, Bodnar RJ (2008) Synthetic fluid inclusions XVII. PVTX properties of high salinity H_2O-NaCl solutions (>30 wt % NaCl): Application to fluid inclusions that homogenize by halite disappearance from porphyry copper and other hydrothermal ore deposits. Econ Geol 103:539–554

Behr HJ, Horn EE, Frentzel-Beyme K, Reutel C (1987) Fluid inclusion characteristics of the Variscan and post-Variscan mineralizing fluids in the Federal Republic of Germany. Chem Geol 61: 273–285

Beshears CJ (2010) The geology and geochemistry of the Millennium deposit, Athabasca Basin, Saskatchewan, Canada. Unpub. MSc thesis, University of Manitoba, 133 p

Boiron MC, Cathelineau M. Banks DA, Buschaert S, Fourcade S, Coulibaly Y, Michelot JL, Boyce A (2002) Fluid transfers at a basement/cover interface: Part II. Large-scale introduction of chlorine into the basement by Mesozoic basinal brines. Chem Geol 192:121–140

Boiron MC, Cathelineau M, Richard A (2010) Fluid flows and metal deposition near basement/cover unconformity: lessons and analogies from Pb–Zn–F–Ba systems for the understanding of Proterozoic U deposits. Geofluids 10:270–292

Bons PD, Fusswinkel T, Gomez-Rivas E, Markl G, Wagner T, Walter B (2014) Fluid mixing from below in unconformity-related ore deposits. Geology 42: 1035–1038

Bodnar RJ (2003) Reequilibration of fluid inclusions. In: Samson I, Anderson A, Marshall D. (eds.), Fluid Inclusions: Analysis and Interpretation. Mineralogical Association of Canada Short Course Series 32, pp. 213–230

Bouch J.E. Naden J. Shepherd TJ, McKervey JA, Young B, Benham AJ, Sloane HJ (2006) Direct evidence of fluid mixing in the formation of stratabound Pb–Zn–Ba–F mineralisation in the Alston Block, North Pennine Orefield (England). Miner Deposita 41:821–835

Card, C., Portella, P., Annesley, I., Pana, D., 2007. Basement rocks to the Athabasca basin. Geological Survey of Canada Bulletin 588, pp. 69–87

Carpenter A.B, Trout ML, Pickett EE (1974) Preliminary report on the origin and chemical evolution of lead- and zinc-rich brines in central Mississippi. Econ Geol 69:1191–1206

Cathelineau M, Boiron MC, Fourcade S, Ruffet G, Clauer N, Belcourt O, Coulibaly Y, Banks DA, Guillocheau F (2012) A major Late Jurassic fluid event at the basin/basement unconformity in western France: $^{40}Ar/^{39}Ar$ and K–Ar dating, fluid chemistry, and related geodynamic context. Chem Geol 322–323:99–120

Chi G, Bosman S, Card C (2013) Numerical modeling of fluid pressure regime in the Athabasca basin and implications for fluid flow models related to the unconformity-type uranium mineralization. J Geochem Explor 125:8–19

Chiarenzelli J, Aspler L, Villeneuve M, Lewry J (1998) Early Proterozoic evolution of the Saskatchewan craton and its allochtonous cover, Trans-Hudson orogen. J Geol 106:247–267

Cloutier J, Kyser K, Olivo GR, Alexandre P, Halaburda J (2009) The Millennium uranium deposit, Athabasca Basin, Saskatchewan, Canada: An atypical basement-hosted unconformity-related uranium deposit. Econ Geol 104: 815–840

Cloutier, J., Kyser, K., Olivo, G., Brisbin, D., 2011. Geochemical, isotopic, and geochronologic constraints on the formation of the Eagle Point basement-hosted uranium deposit, Athabasca Basin, Saskatchewan, Canada and recent remobilization of primary uraninite in secondary structures. Miner Deposita 46, 35–56

Connolly CA, Walter LM, Baadsgaard H, Longstaffe F (1990) Origin and evolution of formation waters, Alberta Basin, Western Canada Sedimentary Basin. 1. Isotope systematics and water mixing. Appl Geochem 5:397–413

Cui T, Yang J, Samson I, (2012a). Tectonic deformation and fluid flow: Implications for the formation of unconformity-related uranium deposits. Econ Geol 107:147–163

Cui T, Yang J, Samson I (2012b) Solute transport across basement/cover interfaces by buoyancy driven thermohaline convection: Implications for the formation of unconformity-related uranium deposits. Am J Sci 312:994–1027

Cumming GL, Krstic D (1992) The age of unconformity-related uranium mineralization in the Athabasca Basin, northern Saskatchewan. Can J Earth Sci 29:1623–1639

Cuney M (2010) Evolution of uranium fractionation processes through time: Driving the secular variation of uranium deposit types. Econ Geol 105:553–569

Dahlkamp FJ (1978) Geologic appraisal of the Key Lake U-Ni deposits, northern Saskatchewan: Econ Geol 73:1430–1449

Dargent M, Dubessy J, Truche L, Bazarkina EF, Nguyen-Trung C, Robert P (2013) Experimental study of uranyl(VI) chloride complex formation in acidic LiCl aqueous solutions under hydrothermal conditions (T = 21°C–350°C, Psat) using Raman spectroscopy. Eur J Mineral 25:765–775

Davisson ML, Criss RE (1996) Na-Ca-Cl relations in basinal fluids. Geochim Cosmochim Acta 60:2743–2752

Derome D, Cathelineau M, Lhomme T, Cuney M (2003) Fluid inclusion evidence of the differential migration of H_2 and O_2 in the McArthur River unconformity-type uranium deposit (Saskatchewan, Canada). Possible role on post-ore modifications of the host rocks. J Geochem Explor 78–79:525–530

Derome D, Cathelineau M, Cuney M, Fabre C, Lhomme T, Banks DA (2005) Mixing of sodic and calcic brines and uranium deposition at the McArthur River, Saskatchewan, Canada. A Raman and laser-induced breakdown spectroscopic study of fluid inclusions. Econ Geol 100:1529–1545

Drever JI (1982) The Geochemistry of Natural Waters. Prentice Hall, Englewood Cliffs, N.J., 338 p

Dubessy J, Derome D, Sausse J (2003) Numerical modelling of fluid mixings in the H_2O-NaCl system. Applications to the North Caramal uranium prospect (Australia). Chem Geol 194:25–39

Earle S, Sopuck V (1989) Regional lithogeochemistry of the eastern part of the Athabasca Basin uranium province, Saskatchewan. In: Muller-Kahle E (ed), Uranium Resources and Geology of North America. International Agency of Nuclear Energy TECHDOC-500, pp. 263–269

Eglinger A, Ferraina C, Tarantola A, André-Mayer AS, Vanderhaeghe O, Boiron MC, Dubessy J, Richard A, Brouand M (2014) Hypersaline fluids generated by high-grade metamorphism of evaporites: fluid inclusion study of uranium occurrences in the Western Zambian Copperbelt. Contrib Mineral Petr 167 in press, doi: 10.1007/s00410-014-0967-9

Essarraj S, Boiron MC, Cathelineau M, Banks DA, Benharref M (2005) Penetration of surface-evaporated brines into the Proterozoic basement and deposition of Co and Ag at Bou Azzer (Morocco): Evidence from fluid inclusions. J Afr Earth Sci 41:25–39

Fayek M. Kyser TK (1997) Characterization of multiple fluid-flow events and rare-earth-element mobility associated with formation of unconformity-type uranium deposits in the Athabasca Basin, Saskatchewan. Can Mineral 35:627–658

Feltrin L, Oliver NHS, Kelso IJ, King S (2003) Basement metal scavenging during basin evolution: Cambrian and Proterozoic interaction at the Century Zn-Pb-Ag Deposit, Northern Australia. J Geochem Explor 78–79:159–162

Fontes JC, Matray JM (1993) Geochemistry and origin of formation brines from the Paris Basin, France 1. Brines associated with Triassic salts. Chem Geol 109:149–175

Freiberger R, Cuney M (2003) New evidence for extensive fluid-circulations within the basement in relation to unconformity type uranium deposit genesis in the Athabasca basin, Saskatchewan, Canada. Proceedings of International Conference Uranium Geochemistry 2003, Nancy, pp. 151–154

Fusswinkel T, Wagner T, Wälle M, Wenzel T, Heinrich CA, Markl G (2013) Fluid mixing forms basement-hosted Pb-Zn deposits: Insight from metal and halogen geochemistry of individual fluid inclusions. Geology 41, 679–682

Gaboreau S, Cuney M, Quirt D, Beaufort D, Patrier P, Mathieu R (2007) Significance of aluminium phosphate-sulfate minerals associated with U unconformity-type deposits: the Athabasca basin, Canada. Am Mineral 92:267–280

Genest S, Robert F, Duhamel I (2010) The Carswell impact event, Saskatchewan, Canada: Evidence for a pre-Athabasca multiring basin? Geol Society Am S 465:543–570

Gleeson S, Yardley BWD, Boyce AJ, Fallick AE, Munz IA (2000) From basin to basement: the movement of surface fluids into the crust. J Geochem Explor 69–70:527–531

Gleeson SA, Yardley BWD, Munz IA, Boyce AJ (2003) Infiltration of basinal fluids into high-grade basement, South Norway: sources and behaviour of waters and brines. Geofluids 3:33–48

Goldstein RH, Reynolds TJ (1994) Systematics of fluid inclusions in diagenetic minerals. Society of Economic Paleontologists and Mineralogists (SEPM) Short Course Volume 31, 198 p

Goldstein RH (2001) Fluid inclusions in sedimentary and diagenetic systems. Lithos 55:159–193

Guillong M, Meier DL, Allan M, Heinrich CA, Yardley BWD (2008) SILLS: A Matlab-based program for the reduction of laser ablation ICP-MS data of homogeneous materials and inclusions. In: Sylvester P (ed.), Laser Ablation ICP–MS in the Earth Sciences: Current Practices and Outstanding Issues. Mineralogical Association of Canada Short Course Series 40, pp. 328–333

Hacini M Oelkers EH (2011) Geochemistry and behavior of trace elements during the complete evaporation of the Merouane Chott ephemeral lake: Southeast Algeria. Aquat Geochem 17:51–70

Hanor JS (1994) Origin of saline fluids in sedimentary basins. In: Parnell J (ed.), Geofluids: Origin, Migration and Evolution of Fluids in Sedimentary Basins. Geol Soc SP 78:151–174

Haynes FM (1985) Determination of fluid inclusion compositions by sequential freezing. Econ Geol 80:1436–1439

Hecht L, Cuney M (2000) Hydrothermal alteration of monazite in the Precambrian crystalline basement of the Athabasca Basin (Saskatchewan, Canada): Implications for the formation of unconformity-related uranium deposits. Miner Deposita 35:791–795

Heine TH (1986) The geology of the Rabbit Lake uranium deposit, Saskatchewan. In: Evans EL (ed.), Uranium deposits of Canada. Canadian institute of Mining, Metallurgy and Petroleum Special Volume 33, pp. 134–143

Hitchon B, Perkins EH, Gunter WD (2001) Recovery of trace metals in formation waters using acid gases from natural gas. Appl Geochem 16:1481–1497

Hodge VF, Johannesson KH, Stetzenbach KJ (1996) Rhenium, molybdenum, and uranium in groundwater from the southern Great Basin, USA. Geochim Cosmochim Acta 60:3197–3214

Hoeve J, Sibbald TII (1978) On the genesis of the Rabbit Lake and other unconformity-type uranium deposits in Northern Saskatchewan, Canada. Econ Geol 73:1450–1473

Hoeve J, Kyser TK, Forester RW (1986) Cover-basement interaction and the origin of U-Ni-Co mineralization in the Athabsca Basin: Isotopic evidence (O, H, C). Saskatchewan Research Council Publication No. R-855-3-A-86. 89 pp

Hoeve J, Quirt DA (1987) A stationary redox front as a critical factor in the formation of high-grade, unconformity-type uranium ores in the Athabasca Basin, Saskatchewan, Canada. B Mineral 110:151–171

Hoffman P (1990) Subdivision of the Churchill Province and extent of the Trans-Hudson Orogen. In: Lewry JF, Stauffer MR (eds.), The Early Proterozoic Trans-Hudson Orogen of North America. Geological Association of Canada Special Paper 37:15–39

Houston S, Smalley C, Laycock A, Yardley BWD (2011) The relative importance of buffering and brine inputs in controlling the abundance of Na and Ca in sedimentary formation waters. Mar Petrol Geol 28:1242–1251

Huizenga JM, Gutzmer J, Banks DA, Greyling L (2006) The Palaeoproterozoic carbonate-hosted Pering Pb-Zn deposit, South Africa. 2: fluid inclusion, fluid chemistry and stable isotope constrains. Miner Deposita 40, 686–706

Hurtig NC, Heinrich CA, Driesner T, Herrmann W, Wall V, Mathison I (2014) Fluid evolution and uranium (-Mo-F) mineralization at the Maureen Deposit (Queensland, Australia): Unconformity-related hydrothermal ore formation with a source in the volcanic cover Sequence. Econ Geol 109: 737–773

Jefferson CW, Thomas DJ, Gandhi SS, Ramaekers P, Delaney G, Brisbin D, Cutts C, Portella P, Olson RA (2007). Unconformity associated uranium deposits of the Athabasca Basin, Saskatchewan and Alberta. Geological Survey of Canada Bulletin 588:23–67

Kendrick MA, Burgess R, Harrison D, Bjorlykke A (2005) Noble gas and halogen evidence for the origin of Scandinavian sandstone-hosted Pb-Zn deposits. Geochim Cosmochim Acta 69:109–129

Kharaka YK, Maest AS, Carothers WW, Law LM, Lamothe PJ, Fries TL (1987) Geochemistry of metal-rich brines from central Mississippi Salt Dome basin, U.S.A. Appl Geochem 2:543–561

Kharaka YK, Hanor JS (2003) Deep Fluids in the Continents: I. Sedimentary Basins. In: Holland HD, Turekian KK (eds.), Treatise on Geochemistry, Volume 5. Elsevier, pp. 499–540

Kister P, Laverret E, Quirt D, Cuney M, Patrier P, Beaufort D, Bruneton P (2006) Mineralogy and geochemistry of the host-rock alterations associated to the Shea Creek unconformity-type uranium deposits (Saskatchewan, Canada), Part 2. Spatial distribution of the Athabasca Group sandstone matrix minerals. Clay Clay Miner 54:295–313

Kraemer TF, Kharaka YK (1986) Uranium geochemistry in geopressured-geothermal aquifers of the U.S. Gulf Coast. Geochim Cosmochim Acta 50:1233–1238

Kovalevych VM, Marshall T, Peryt TM, Petrychenko OY, Zhukova SA (2006) Chemical composition of seawater in Neoproterozoic: Results of fluid inclusion study of halite from Salt Range (Pakistan) and Amadeus Basin (Australia). Precambrian Res 144:39–51

Kotzer TG, Kyser TK, Irving E (1992) Paleomagnetism and the evolution of fluids in the Proterozoic Athabasca Basin, Northern Saskatchewan, Canada. Can J Earth Sci 29:1474–1491

Kotzer TG, Kyser TK (1995) Petrogenesis of the Proterozoic Athabasca Basin, Northern Saskatchewan, Canada, and its relation to diagenesis, hydrothemal uranium mineralization and paleohydrogeology. Chem Geol 120:45–89

Koziy L, Bull S, Large R, Selley D (2009) Salt as a fluid driver, and basement as a metal source, for stratiform sediment-hosted copper deposits. Geology 37:1107–1110

Ku, TL, Knauss KG, Mathieu GG (1977) Uranium in open ocean: concentration and isotopic composition. Deep Sea Research 24:1005–1117.

Kyser TK, Hiatt E, Renac C, Durocher K, Holk G, Deckart K (2000) Diagenetic fluids in paleo- and meso-proterozoic sedimentary basins and their implications for long protracted fluid histories. In: Kyser K. (ed.), Fluids and basin evolution. Mineralogical association of Canada Short Course Series 28, pp. 225–262

Kyser TK, Cuney M (2008) Unconformity-related uranium deposits. In: Cuney M, Kyser K (eds.), Recent and Not-So-Recent Developments in Uranium Deposits and Implications for Exploration. Mineralogical Association of Canada Short Course Series 39, pp. 161–219

Land LS, Macpherson GL (1992) Origin of saline formation waters, Cenozoic section, Gulf of Mexico sedimentary basin. Am Assoc Petr Geol B 76:1344–1362

Lawler JP, Crawford ML (1982) Fluid inclusions in the Midwest Lake Uranium deposit. Geological Society of America, Abstracts with Programs 14, pp. 542

Leisen M, Boiron MC, Richard A, Dubessy J (2012) Determination of Cl and Br concentrations in individual fluid inclusions by combining microthermometry and LA-ICPMS analysis: Implications for the origin of salinity in crustal fluids. Chem Geol, 330–331:197–206

Lorilleux G, Jébrak M, Cuney M, Baudemont D (2002) Polyphase hydrothermal breccia associated with unconformity-related uranium mineralizations (Canada). From fractal analysis to structural significance. J Struct Geol 24:323–338

Lorilleux G, Cuney M, Jébrak M, Rippert JC, Portella P (2003) Chemical brecciation processes in the Sue unconformity-type uranium deposits, Eastern Athabasca Basin (Canada). J Geochem Explor 80:241–258

Longerich HP, Jackson SE, Günther D (1996) Laser ablation inductively coupled plasma mass spectrometric transient signal data acquisition and analyte concentration calculation. J Anal Atom Spectrom 11:899–904

Lowenstein TK, Timofeeff MN, Brennan ST, Hardie LA, Demicco RV (2001) Oscillations in Phanerozoic seawater chemistry: Evidence from fluid inclusions. Science 294:1086–1088

Lowenstein TK, Timofeeff MN (2008) Secular variations in seawater chemistry as a control on the chemistry of basinal brines: test of the hypothesis. Geofluids 8:77–92

McGowan RR, Roberts S, Boyce AJ (2006) Origin of the Nchanga copper-cobalt deposits of the Zambian Copperbelt. Miner Deposita 40:617–638

Mercadier J, Richard A, Boiron MC, Cathelineau M, Cuney M (2010) Brine migration in the basement rocks of the Athabasca Basin through microfracture networks (P-Patch U deposit, Canada). Lithos 115:121–136

Mercadier J, Cuney M, Cathelineau M, Lacorde M (2011a) U redox fronts and kaolinisation in basement-hosted unconformity-related U ores of the Athabasca Basin (Canada): late U remobilisation by meteoric fluids. Miner Deposita 46:105–135

Mercadier J, Cuney M, Lach P, Boiron MC, Bonhoure J, Richard A, Leisen M, Kister P (2011b) Origin of uranium deposits revealed by their rare earth element signature. Terra Nova 23:264–269

Mercadier J, Richard A, Cathelineau M (2012) Boron- and magnesium-rich marine brines at the origin of giant unconformity-related uranium deposits: δ^{11}B evidence from Mg-tourmalines. Geology 40:231–234

Mercadier J, Annesley IR, McKechnie CL, Bogdan TS, Creighton S (2013) Magmatic and metamorphic uraninite mineralization in the western margin of the Trans-Hudson Orogen (Saskatchewan, Canada): a uranium source for unconformity-related uranium deposits? Econ Geol 108, 1037–1065

Muchez P, Heijlen W, Banks DA, Blundell D, Boni M, Grandia F (2005) Extensional tectonics and the timing and formation of basin-hosted deposits in Europe. Ore Geol Rev 27:241–267

Munz IA, Yardley BWD, Banks DA, Wayne DW (1995) Deep penetration of sedimentary fluids in basement rocks from southern Norway: Evidence from hydrocarbon and brine inclusions. Geochim Cosmochim Acta 59:239–254

Ng R, Alexandre P, Kyser K (2013) Mineralogical and Geochemical Evolution of the Unconformity-Related McArthur River Zone 4 Orebody in the Athabasca Basin, Canada: Implications of a Silicified Zone. Econ Geol 108:1657–1689

Oliver NHS, McLellan JG, Hobbs BE, Cleverly JS, Ord A, Feltrin L (2006) Numerical models of extensional deformation, heat transfer, and fluid flow across basement-cover interfaces during basin-related mineralization. Econ Geol 101:1–31

Pagel M (1975a) Cadre Géologique des gisements d’uranium dans la structure Carswell (Saskatchewan – Canada) – « Etude des phases fluides ». Unpub. PhD thesis, Université de Nancy 1, 157 p

Pagel M (1975b) Détermination des conditions physico-chimiques de la silicification diagénétique des grès Athabasca (Canada) au moyen des inclusions fluides. Comptes Rendus de l’Académie des Sciences de Paris 280:2301–2304

Pagel M, Poty B, Sheppard SMF (1980) Contribution to some Saskatchewan uranium deposits mainly from fluid inclusion and isotopic data. In: IAEA (ed.), International Uranium Symposium on the Pine Creek Geosyncline, Vienna, pp. 639–654

Pagel M, Wheatley K, Ey F (1985) Origin of the Carswell circular structure. A summary of data for geological interpretation of its formation. In: Laine R, Alonso D, Svab M (eds.), The Carswell Structure Uranium Deposits Saskatchewan. Geological Association of Canada Special Paper 29, pp. 213–223

Pagel M, Ahamdach N (1995) Etude des inclusions fluides dans les quartz des gisements d'uranium de l'Athabasca et du Thelon (Canada). CREGU internal report, 9 p

Piqué A, Canals A, Grandia F, Banks DA (2008) Mesozoic fluorite veins in NE Spain record regional base metal-rich brine circulation through basin and basement during extensional events. Chem Geol 257:139–152

Pluta I, Zuber A (1995) Origin of brines in the Upper Silesian Coal Basin (Poland) inferred from stable isotope and chemical data. Appl Geochem 10:447–460

Poty B, Pagel M (1988) Fluid inclusions related to uranium deposits: a review. Journal of the Geological Society of London 145:157–162

Quirt D (2003) Athabasca unconformity-type uranium deposits: one type of deposit with many variations. Proceedings of International Conference Uranium Geochemistry 2003, Nancy, pp. 309–312

Raffensperger JP, Garven G (1995) The formation of unconformity-type uranium ore deposits 2. Coupled hydrochemical modeling. Am J Sci 295:639–696

Ramaekers P, Jefferson CW, Yeo GM, Collier B, Long DG, Catuneanu O, Bernier S, Kupsch B, Post R, Drever G, McHardy S, Jircka D, Cutts C, Wheatley K (2007) Revised geological map and stratigraphy of the Athabasca Group, Saskatchewan and Alberta. Geological Survey of Canada Bulletin 588:155–191

Richard A, Pettke T, Cathelineau M, Boiron MC, Mercadier J, Cuney M, Derome D (2010) Brine-rock interaction in the Athabasca basement (McArthur River U deposit, Canada): consequences for fluid chemistry and uranium uptake. Terra Nova 22:303–308

Richard A, Banks DA, Mercadier J, Boiron MC, Cuney M, Cathelineau M (2011) An evaporated seawater origin for the ore-forming brines in unconformity-related uranium deposits (Athabasca Basin, Canada): Cl/Br and δ^{37}Cl study of fluid inclusions. Geochim Cosmochim Acta 75:2792–2810

Richard A, Rozsypal C, Mercadier J, Banks DA, Cuney M, Boiron MC, Cathelineau M (2012) Giant uranium deposits formed from exceptionally uranium-rich acidic brines. Nat Geosci 5:142–146

Richard A, Cauzid J, Cathelineau M, Boiron MC, Mercadier J, Cuney M (2013a) Synchrotron-XRF and XANES investigation of uranium speciation and element distribution in fluid inclusions from unconformity-related uranium deposits. Geofluids 13:101–111

Richard A, Boulvais P, Mercadier J, Boiron MC, Cathelineau M, Cuney M, France-Lanord C (2013b). From evaporated seawater to uranium-mineralizing brines: Isotopic and trace element study of quartz-dolomite veins in the Athabasca system. Geochim Cosmochim Acta 113:38–59

Richard A, Kendrick MA, Cathelineau M (2014) Noble gases (Ar, Kr, Xe) and halogens (Cl, Br, I) in fluid inclusions from the Athabasca Basin (Canada): Implications for unconformity-related U deposits. Precambrian Res 247:110‒125

Ruzicka V (1989) Monometallic and polymetallic deposits associated with sub-Athabasca unconformity in Saskatchewan. Geological Survey of Canada Paper 1–C, 67–79

Sánchez V, Vindel E, Martin-Crespo T, Corbella M, Cardellach E, Banks DA (2009) Sources and composition of fluids associated with fluorite deposits of Asturias (N Spain). Geofluids 9:338–355

Scott R, Chi G, Bosman SA (2011) A petrographic and fluid inclusion study of the Athabasca Group sandstones from Rumpel Lake drill core, Athabasca Basin, northern Saskatchewan. In: Summary of investigations 2011, Volume 2. Saskatchewan Geological Survey, Saskatchewan Ministry of Energy and Resources, Miscellaneous Report 2011-4.2 paper A-5, 10p

Shelton KL, Burstein IB, Hagni RD, Vierrether CB, Grant SK, Hennigh QT, Bradley MF, Brandom RT (1995) Sulfur isotope evidence for penetration of MVT fluids into igneous basement rocks, southeast Missouri, USA. Miner Deposita 30:339–350

Shepherd TJ, Chenery SR (1995) Laser ablation ICP-MS elemental analysis of individual fluid inclusions: An evaluation study. Geochim Cosmochim Acta 59:3997–4007

Steele-MacInnis M, Bodnar RJ, Naden J (2011) Numerical model to determine the composition of H_2O-NaCl-$CaCl_2$ fluid inclusions based on microthermometric and microanalytical data. Geochim Cosmochim Acta 75:21–40

Stoffell B, Wilkinson JJ, Jeffries TE (2004) Metal transport and deposition in hydrothermal veins revealed by 213nm UV laser ablation microanalysis of single fluid inclusions. Am J Sci 304:533–557

Stoffell B, Appold MS, Wilkinson JJ, McClean NA, Jeffries TE (2008) Geochemistry and evolution of Mississippi Valley-type mineralizing brines from the Tri-State and Northern Arkansas districts determined by LA-ICP-MS microanalysis of fluid Inclusions. Econ Geol 103:1411–1435

Stueber AM, Walter LM (1991) Origin and chemical evolution of formation waters from Silurian-Devonian strata in the Illinois basin, USA. Geochim Cosmochim Acta 55:309–325

Sverjensky DA (1984) Oil field brines as ore-forming solutions. Econ Geol 79:23–37

Sverjensky DA (1989) Chemical evolution of basinal brines that formed sediment-hosted Cu-Pb-Zn deposits. In: Boyle RW, Brown AC, Jefferson CJ, Jowett EC, Kirkham RV (eds.), Sediment

Hosted Stratiform Copper deposits. Geological Association of Canada Special Paper 36:127–134

Swarbrick RE, Osborne MJ (1997) Mechanisms for generating overpressure in sedimentary basins: A reevaluation. Am Assoc Petr Geol B 81:1023–1041

Vanko DA, Bodnar RJ, Sterner SM (1988) Synthetic fluid inclusions: VIII. Vapor-saturated halite solubility in part of the system NaCl-$CaCl_2$-H_2O, with application to fluid inclusions from oceanic hydrothermal systems. Geochim Cosmochim Acta 52:2451–2456

Warren JK (1997) Evaporites, brines and base metals: Fluids, flow and 'the evaporite that was'. Aust J Earth Sci 44:149–183

Wilkinson JJ, Everett CE, Boyce AJ, Gleeson SA, Rye DM (2005) Intracratonic crustal seawater circulation and the genesis of subseafloor zinc-lead mineralization in the Irish orefield. Geology 33:805–808

Wilkinson JJ, Stoffell B, Wilkinson CC, Jeffries TE, Appold MS (2009) Anomalously metal-rich fluids form hydrothermal ore deposits. Science 323:764–767

Wilson MR, Kyser TK (1987) Stable isotope geochemistry of alteration associated with the Key Lake uranium deposit, Canada. Econ Geol 82:1540–1557

Wilson MR, Kyser TK, Mehnert HH, Hoeve J (1987) Changes in the H-O-Ar isotope composition of clays during retrograde alteration. Geochim Cosmochim Acta 51:869–878

Worden RH, Manning DAC, Bottrell SH (2006) Multiple generations of high salinity formation water in the Triassic Sherwood Sandstone: Wytch Farm oilfield, onshore UK. Appl Geochem 21:455–475

Yardley BWD (2005) 100th Anniversary Special Paper: Metal concentrations in crustal fluids and their relationship to ore formation. Econ Geol 100:613–632

Zhang YG, Frantz JD.(1987) Determination of the homogenization temperatures and densities of supercritical fluids in the system NaCl-KCl-$CaCl_2$-H_2O using synthetic fluid inclusions. Chem Geol 64:335–350

Zwart EW, Touret JLR (1994) Melting behavior and composition of aqueous fluid inclusions in fluorite and calcite: applications within the system H_2O-$CaCl_2$-NaCl. Eur J Mineral 6:773–786

Table captions

Table 1: Fluid inclusion nomenclature and summary fluid inclusion data for the McArthur River deposit, after Derome et al. (2005) and Richard et al. (2010). LA-ICP-MS: laser ablation-inductively coupled plasma-mass spectrometry; hyd.: hydrohalite; Te: eutectic melting; Tm ice: ice melting; Tm hyd: hydrohalite melting; Ts NaCl: halite dissolution; Th: homogenization to the vapor phase; LIBS: laser-induced breakdown spectroscopy. Lw' and Lwh' inclusions frequently fail to nucleate any ice upon cooling, and only observed Tm ice ranges are reported.

Table 2: Summary of fluid inclusion types previously described in the Athabasca Basin and Basement. Fluid inclusion microthermometric data from previous studies were compiled and fluid inclusions classified based on the nomenclature used in Derome et al. (2005), Richard et al. (2010) and Mercadier et al. (2010); see Section “Fluid inclusion nomenclature and previous studies” for details. Only primary or pseudosecondary fluid inclusions are considered here except for secondary fluid inclusions in magmatic and metamorphic quartz from basement rocks. References are as follows: 1: Derome et al. 2005; 2: Richard et al. 2010; 3: Kotzer and Kyser 1995; 4: Pagel and Ahamdach 1995; 5: Mercadier et al. 2010; 6:

Pagel et al. 1980; 7: Freiberger et al. 2003; 8: Lawler and Crawford 1982; 9: Pagel 1975a; 10: Pagel 1975b; 11: Pagel and Ahamdach 1995; 12: Scott et al. 2011; 13: Beshears 2010; 14: Poty and Pagel 1988.

Figure captions

Fig. 1: (A) Simplified geological map of the Athabasca Basin and Basement, Canada, modified from Jefferson et al. (2007). Circles indicate the locations of the main uranium deposits (including those mentioned in Table 3 with the exception of Rumpel Lake, where only typical alteration is described but no mineralization. Large red circles represent the uranium deposits studied in this work. Basement domains are identified by different shades of grey. TMZ: Thelon magmatic zone; WMTZ: Wollaston Mudjatik transition zone; VRSZ: Virgin River shear zone; BLSZ: Black Lake shear zone. The Snowbird Tectonic Zone separates the Rae Subprovince in the west from the Hearne Subprovince in the east. (B) Simplified mineral paragenesis for unconformity-related U deposits in the Athabasca Basin and Basement. Alteration types (E: early diagenetic, hydrothermal and late meteoric) are indicated. Diag.: diagenetic. Modified from Kotzer and Kyser (1995), Derome et al. (2005) and Kyser and Cuney (2008) for early diagenetic and hydrothermal events, and Mercadier et al. (2011a) for late meteoric events.

Fig. 2: Examples of fluid-inclusion-hosting quartz and dolomite veins studied in this work. (A) Hematite-dolomite vein cross-cutting a biotite-rich gneiss (sample H1935-8, Eagle Point). (B) Quartz ± hematite veins cross-cutting a hematite-rich gneiss (sample ERC5-922.0, Shea Creek). (C) Quartz-dolomite vein cross-cutting a hematite-rich gneiss (sample RBL2Qz, Rabbit Lake). (D) Quartz-dolomite vein cross-cutting “bleached” (illite-chlorite-dravite

alteration) gneiss (sample CX52-1, Millennium). (E) Quartz vein cross-cutting “bleached” gneiss (sample P48-5, P-Patch). (F) Primary two-phase (liquid + vapor) fluid inclusions aligned along a dolomite growth band (highlighted by white dashed lines). (G) Cluster of primary and pseudosecondary two-phase (liquid + vapor) fluid inclusions. Pseudosecondary fluid inclusions planes are highlighted by black dashed lines. A quartz growth band is highlighted by a white dashed line. In such cases, primary and pseudosecondary inclusions are petrographically nearly indistinguishable. (H) Three-phase (liquid-vapor-halite) primary inclusion in quartz, showing negative crystal shape. Further illustration of fluid inclusions and quartz-dolomite veins, breccias and cements from McArthur River, Rabbit Lake, P-Patch and Millennium, can be found in Pagel et al. 1980; Kotzer and Kyser 1995; Derome et al. 2005; Mercadier et al. 2010; Beshears 2010; Richard et al. 2010, 2011, 2012).

Fig. 3: Fluid inclusion compositions in the ternary H_2O-NaCl-$CaCl_2$ system from microthermometric data for the Rabbit Lake (A), Eagle Point (B), Shea Creek (C), P-Patch (D) and Millennium (E) deposits, together with data for the McArthur River deposit (F) from Derome et al. (2005). (G) Compilation of data from all deposits. (H) Possible compositional fields for the different fluid-inclusion types. Ternary diagrams have been modified from Vanko et al. (1988).

Fig. 4: Ice melting temperature (Tm ice) - Homogenization temperature (Th) relationships of the quartz-hosted Athabasca fluid inclusions for the P-Patch, Eagle Point, Shea Creek and Rabbit Lake deposits, together with data for the McArthur River deposit from Derome et al. (2005).

Fig. 5: Ice melting temperature (Tm ice) - Homogenization temperature (Th) relationships of the dolomite-hosted Athabasca fluid inclusions for the Rabbit Lake, Eagle Point and P-Patch deposits.

Fig. 6: Homogenization temperature (Th) - Halite dissolution temperature (Ts NaCl) - phase volume relationships of the Athabasca fluid inclusions for the P-Patch, Eagle Point, Shea Creek and Rabbit Lake deposits, together with data for the McArthur River deposit from Derome et al. (2005). (A) Ts NaCl vs Th for quartz- and dolomite-hosted fluid inclusions. Note that Lwh' inclusions were not found in dolomite. (B) Distribution of Δ(Ts NaCl - Th) values as a function of the volumetric relationship between NaCl and the vapor phase in the fluid inclusions. V(vap): volume of the vapor phase; V(NaCl): volume of the NaCl phase.

Fig. 7: LA-ICP-MS data for individual quartz-hosted fluid inclusions from the Rabbit Lake, P-Patch, Eagle Point, Millennium and McArthur River deposits. Data for McArthur River after Richard et al. (2010). Stars indicate the possible composition of epsomite-saturated evaporated seawater from which the NaCl-rich and $CaCl_2$-rich brines originated (see Section "Origin and behavior of major solutes and metals" for details). Red stars ($MgSO_4$ seas) after Fontes and Matray (1993). Blue stars ($CaCl_2$ seas) after Lowenstein and Timofeef (2008). Arrows indicate the expected directions of compositional shifts for the following reactions: Mix. with hal.-diss. brine: mixing with halite-dissolution brine; Dol.: dolomitization of calcite; Alb. Pl.: albitization of plagioclase; Alb. KFs.: Albitization of K-feldspar; Mg-alt.: Mg alteration (sudoite, dravite).

Fig. 8: Ranges of element concentrations for the NaCl-rich brine and $CaCl_2$-rich brine end-members from LA-ICP-MS data. The NaCl-rich brine end-member is defined by fluid inclusions with Na > 80000 ppm. The $CaCl_2$-rich brine end-member is defined by fluid inclusions with Na <

30000 ppm. Boxplots show 10th and 90th percentiles (whiskers), 25th and 75th percentiles (box edges) and the median (inner bar).

Fig. 9: Possible P-T reconstruction of the Athabasca brines under static geothermal gradient condition. Representative isochores have been drawn from the most representative range of homogenization temperatures (Th) in both quartz and dolomite. The possible P-T field for the NaCl-rich brine end-member (i.e. before mixing) is ~180 ± 30°C and ~800 ± 400 bars. The possible P-T field for the $CaCl_2$-rich brine end-member (i.e. before mixing) is ~120 ± 30°C and ~600 ± 300 bars). The hydrostatic and lithostatic pressures at 3 and 6 km depth are reported as well as the hydrostatic and lithostatic gradients calculated for thermal gradients of 30°, 35°, and 40°C/km.

Fig. 10: Ranges of metal concentrations in sedimentary formation brines (from boreholes, after Carpenter et al. 1974; Kraemer and Kharaka 1986; Kharaka et al. 1987; Banner et al. 1990; Connolly et al. 1990; Stueber and Walter 1991; Land and Macpherson 1992; Pluta and Zuber 1995; Hodge et al. 1996; Hitchon et al. 2001; Aquilina et al. 2002) and ore fluids from basin-hosted base metal (Pb, Zn, Ba) deposits (from LA-ICP-MS analysis of fluid inclusions, after Appold et al. 2004; Stoffell et al. 2004; Bouch et al. 2006; Huizenga et al. 2006; Piqué et al. 2008; Stoffell et al. 2008; Sanchez et al. 2009; Wilkinson et al. 2009; Appold and Wenz 2011) and Athabasca fluid inclusions (this study). Boxplots show 5th and 95th percentiles (symbols), 10th and 90th percentiles (whiskers), 25th and 75th percentiles (box edges) and the median (inner bar). (1) Typical limits of detection for LA-ICP-MS analysis of metals in fluid inclusions. Black solid lines represent the ranges of the highest values for metal concentrations in each of the selected studies. Grey dotted lines represent the lower ranges of metal concentrations in the selected studies.

Figure 1

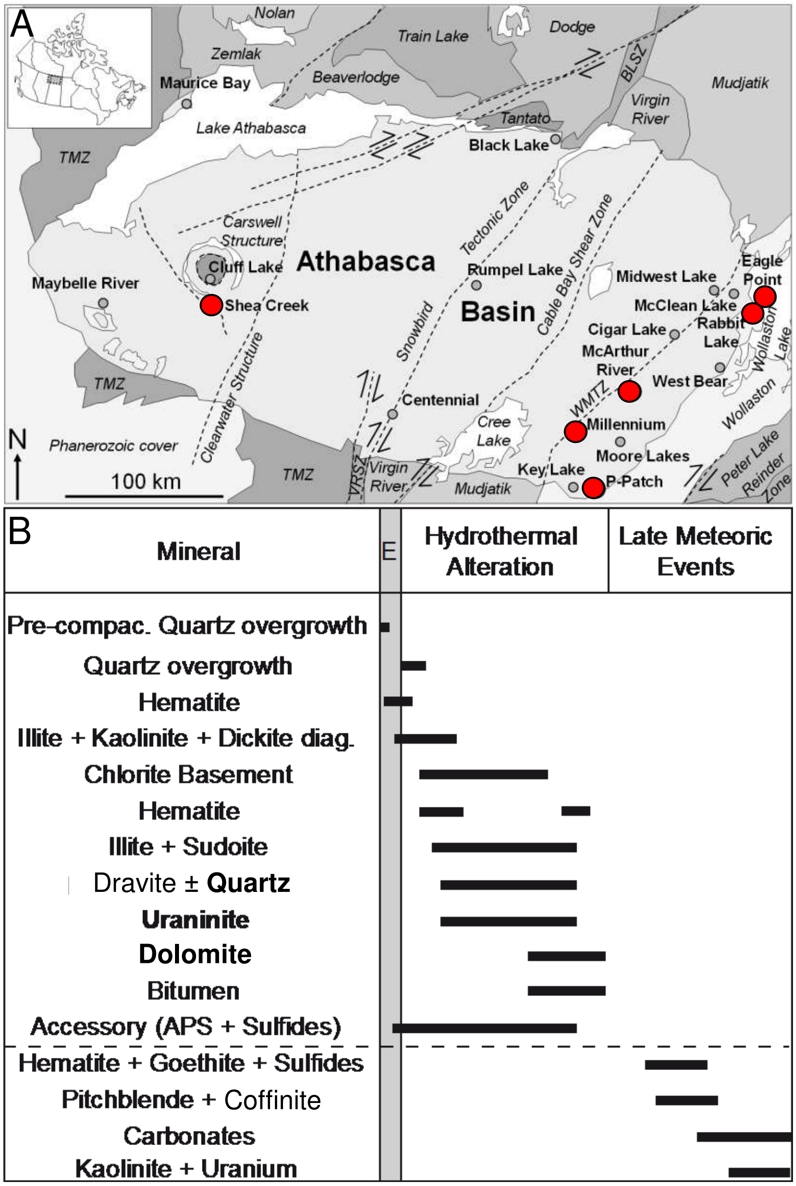

FIGURE 1

Figure 2

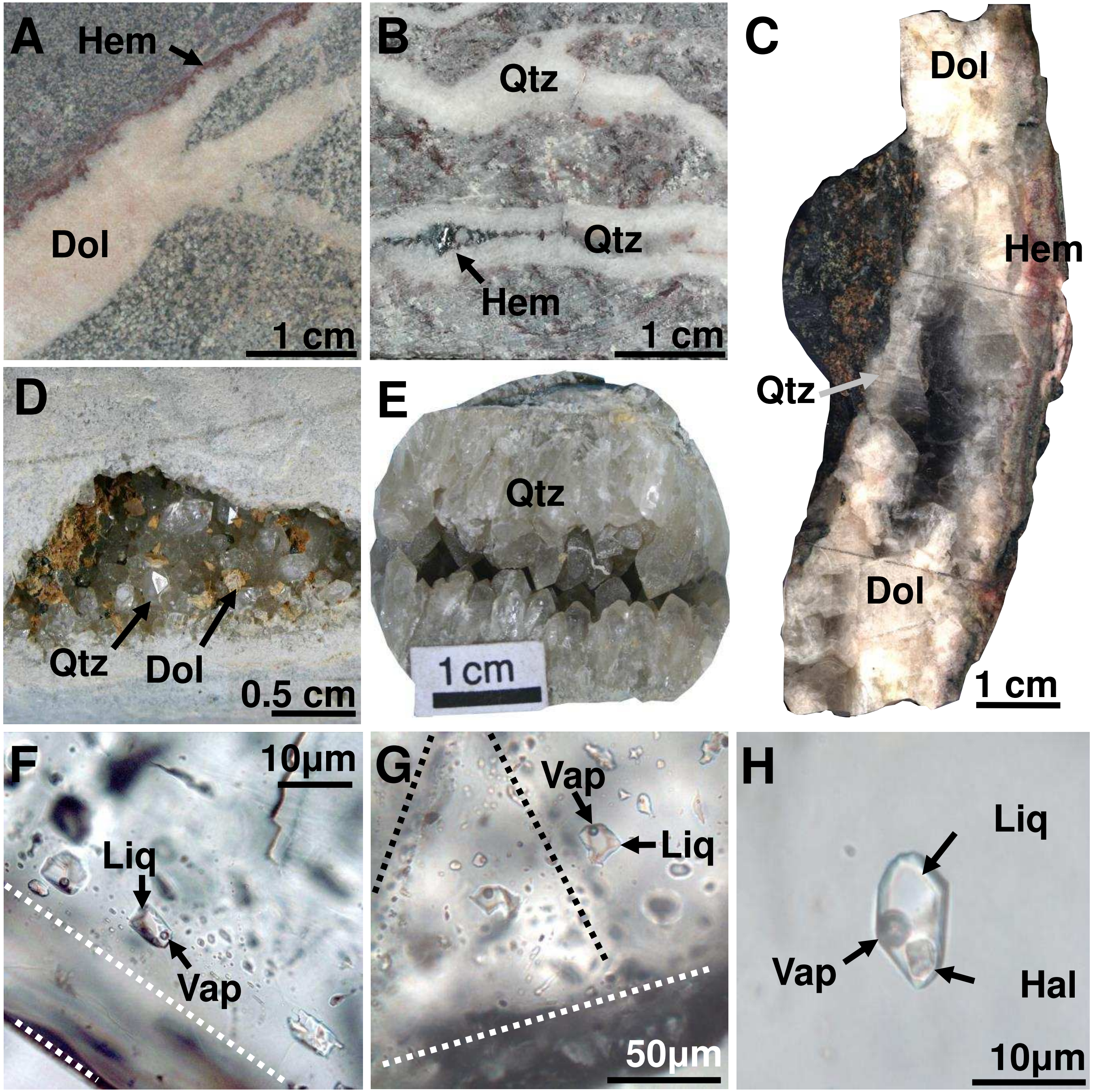

FIGURE 2

Figure 3

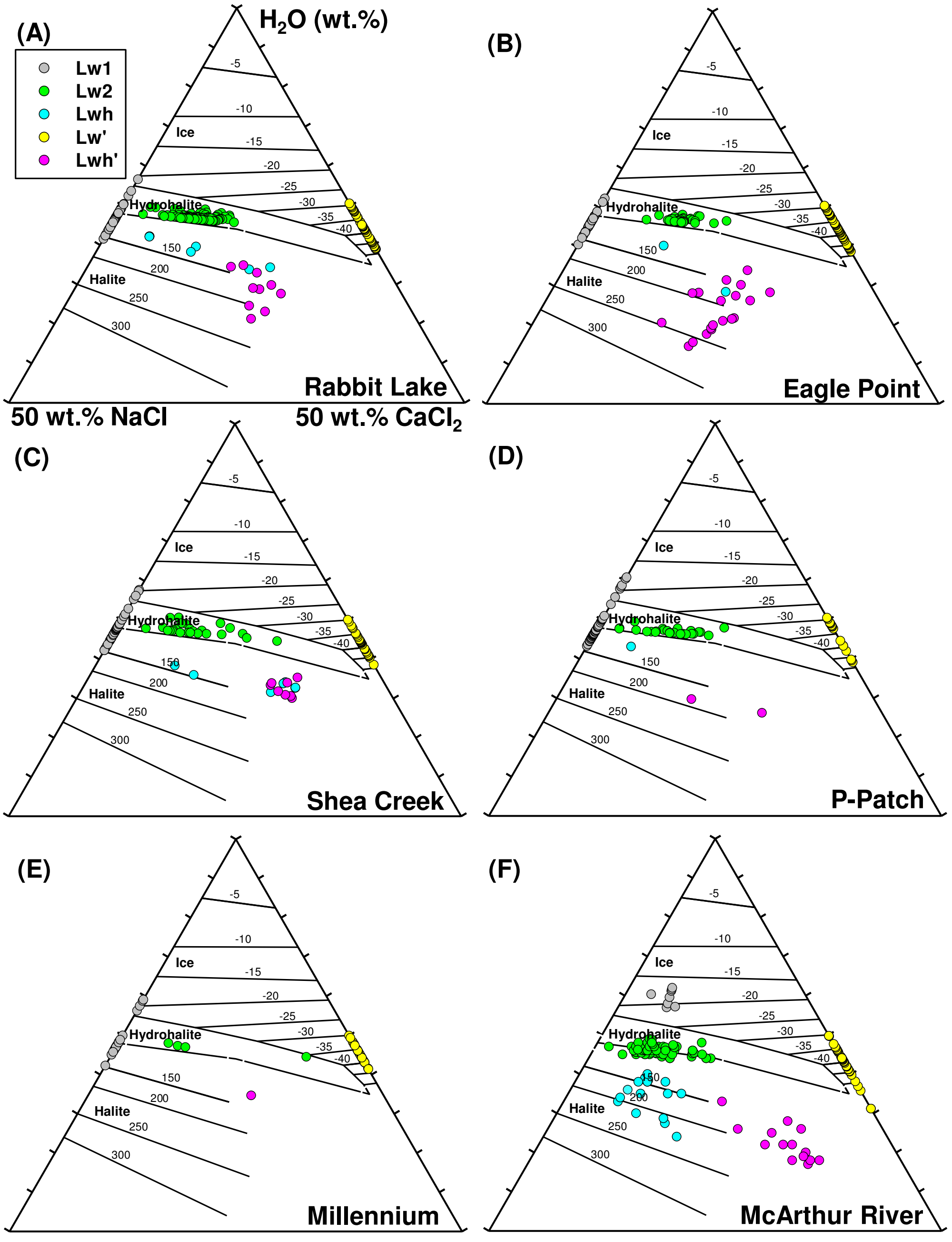

FIGURE 3 (continued on the next page)

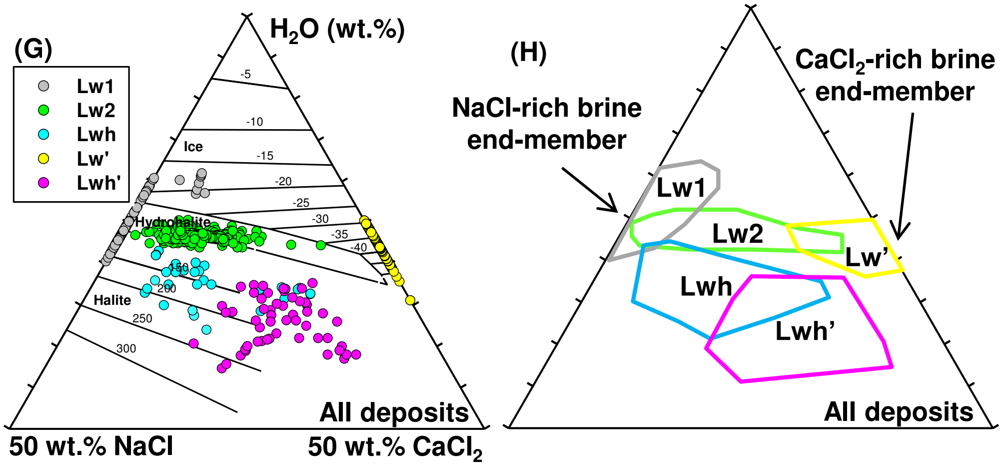
(G)
Lw1
Lw2
Lwh
Lw'
Lwh'
H_2O (wt.%)
-5
-10
Ice
-15
-20
-25
-30
-35
-40
Hydrohalite
150
200
Halite
250
300
All deposits
50 wt.% NaCl
50 wt.% $CaCl_2$
(H)
NaCl-rich brine end-member
$CaCl_2$-rich brine end-member
Lw1
Lw2
Lw'
Lwh
Lwh'
All deposits

FIGURE 3

Figure 4

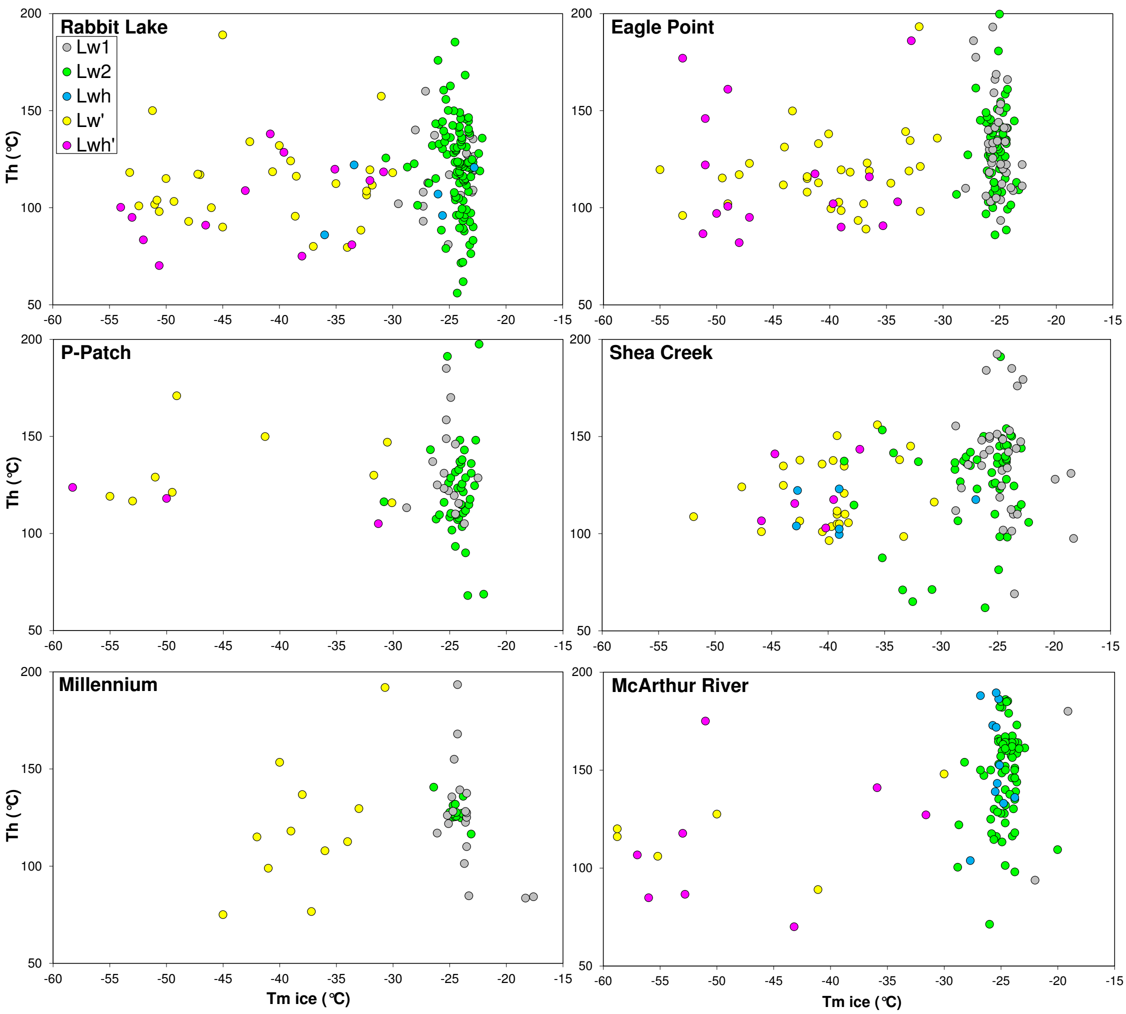

FIGURE 4

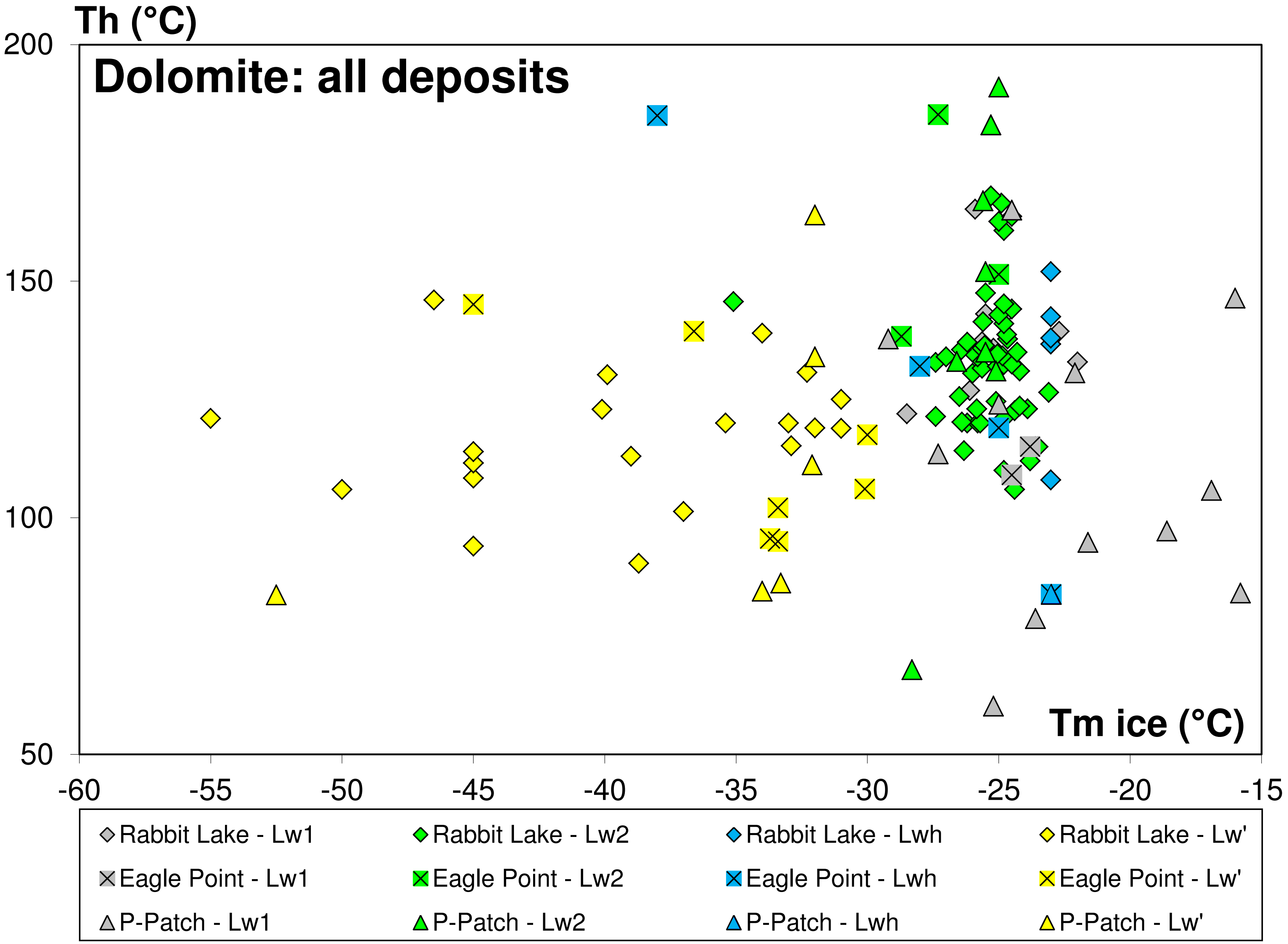
Th (°C)
Dolomite: all deposits
200
150
100
50
-60
-55
-50
-45
-40
-35
-30
-25
-20
-15
Tm ice (°C)
Rabbit Lake - Lw1
Rabbit Lake - Lw2
Rabbit Lake - Lwh
Rabbit Lake - Lw'
Eagle Point - Lw1
Eagle Point - Lw2
Eagle Point - Lwh
Eagle Point - Lw'
P-Patch - Lw1
P-Patch - Lw2
P-Patch - Lwh
P-Patch - Lw'

FIGURE 5

Figure 6

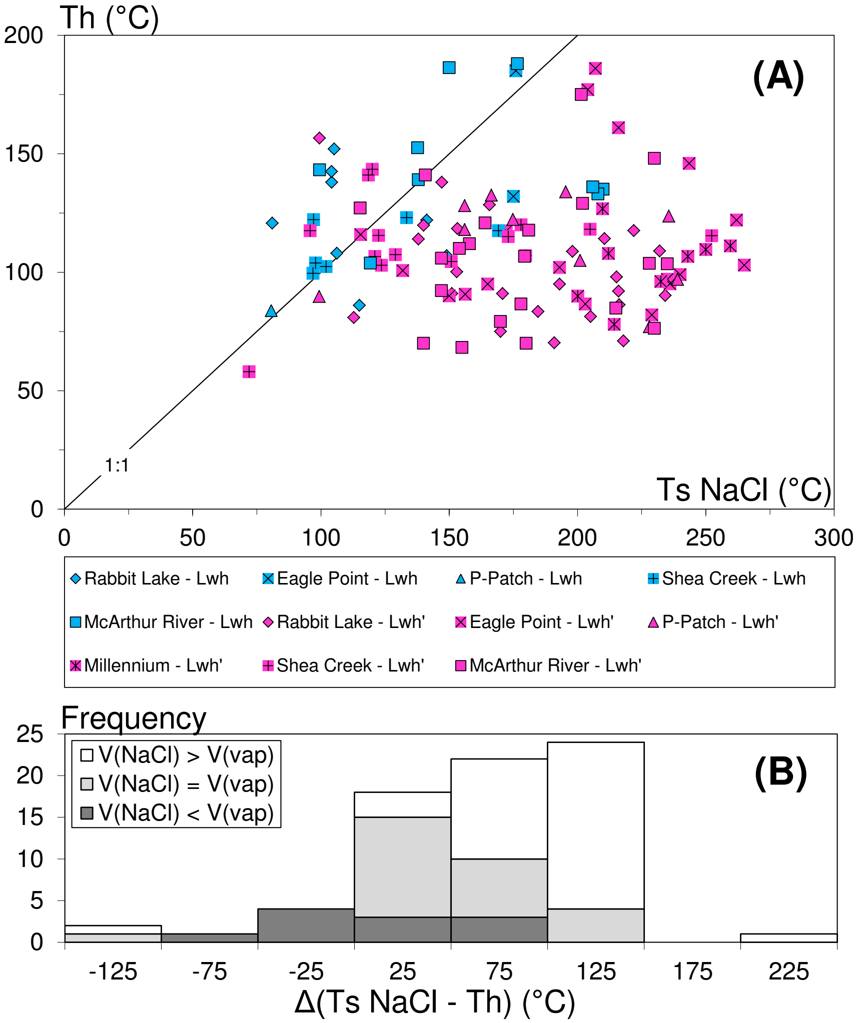

FIGURE 6

Figure 7 (one page)

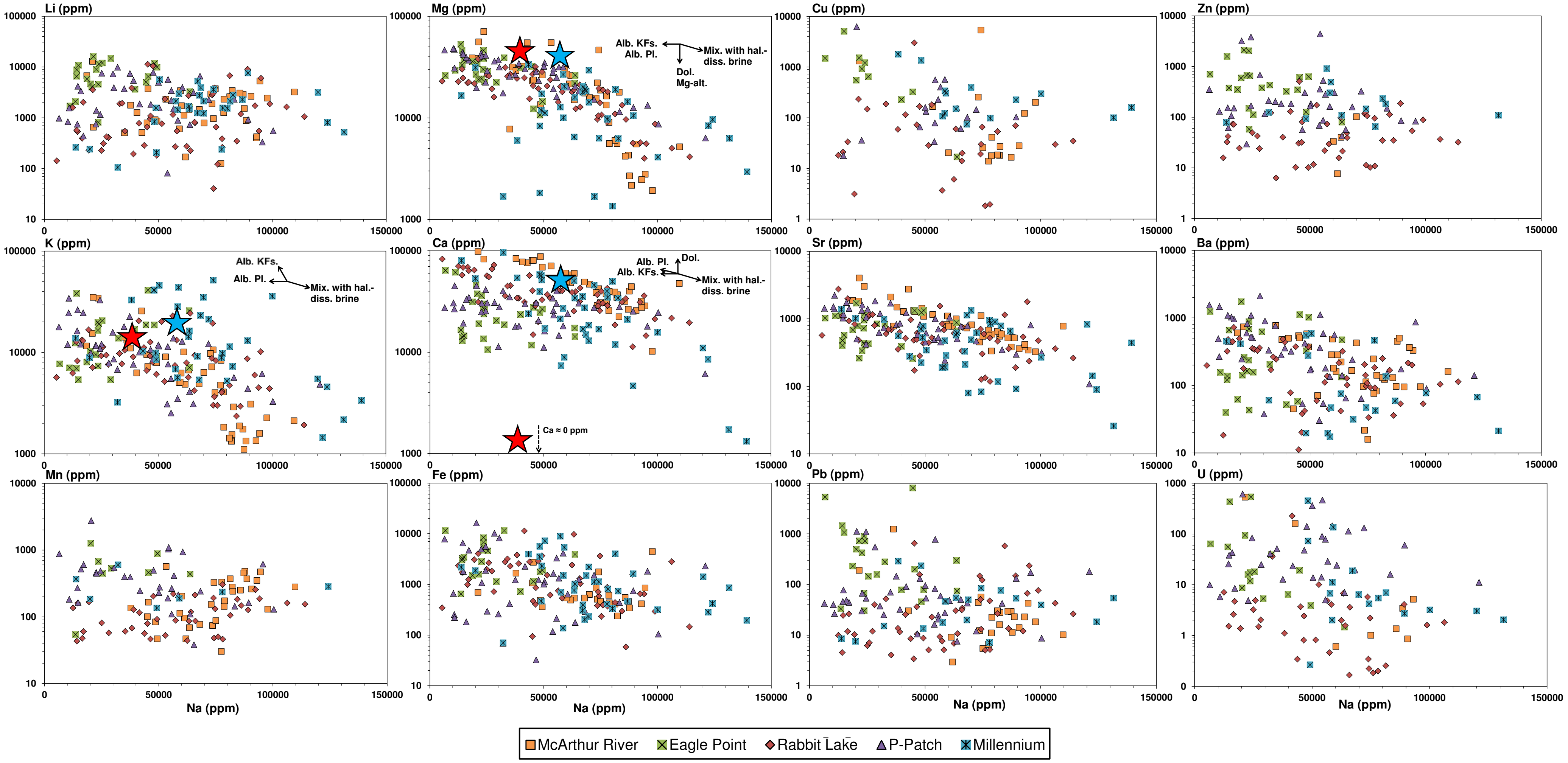

FIGURE 7

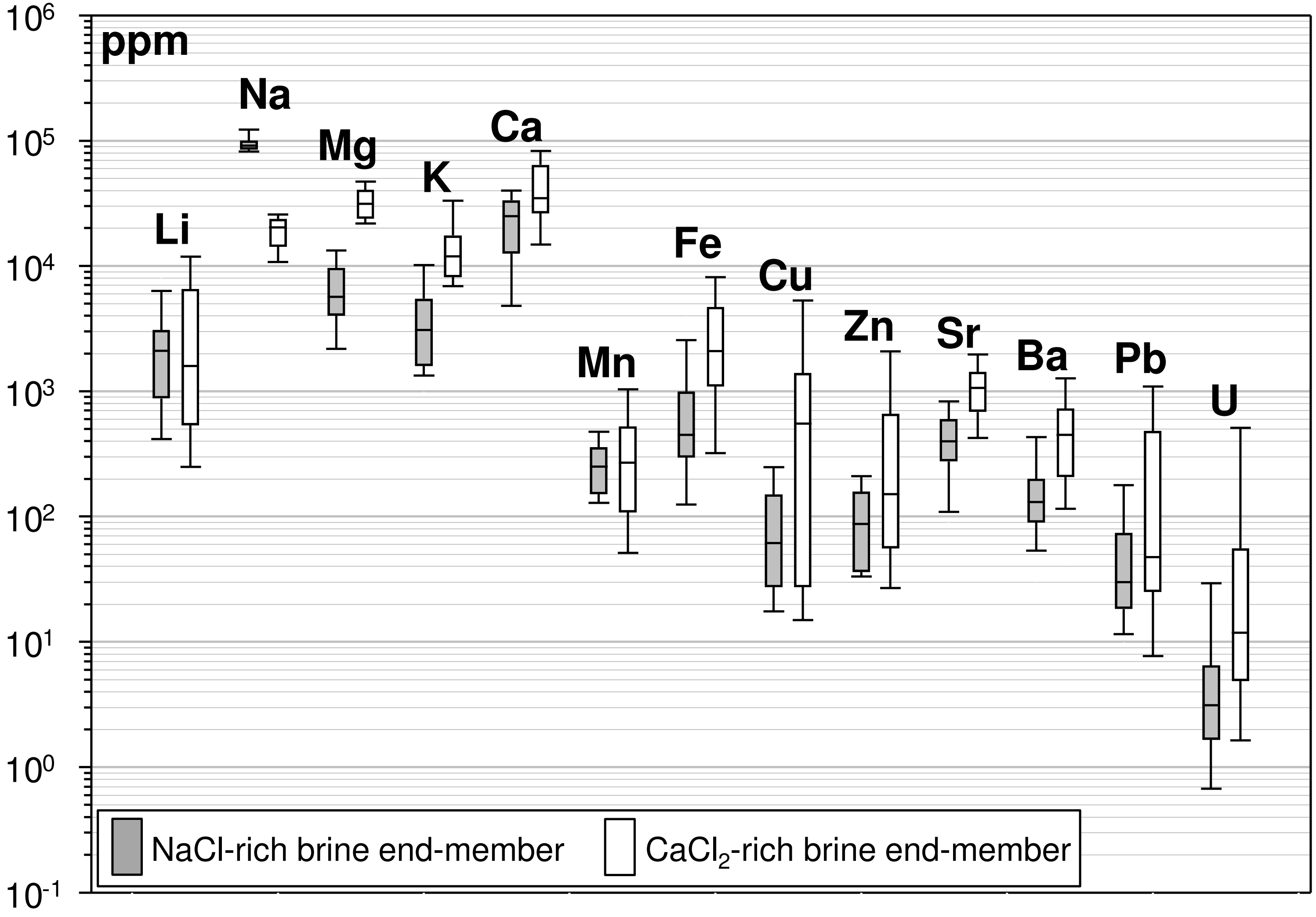
10^6
10^5
10^4
10^3
10^2
10^1
10^0
10^-1
ppm
Li
Na
Mg
K
Ca
Mn
Fe
Cu
Zn
Sr
Ba
Pb
U
NaCl-rich brine end-member
CaCl2-rich brine end-member

FIGURE 8

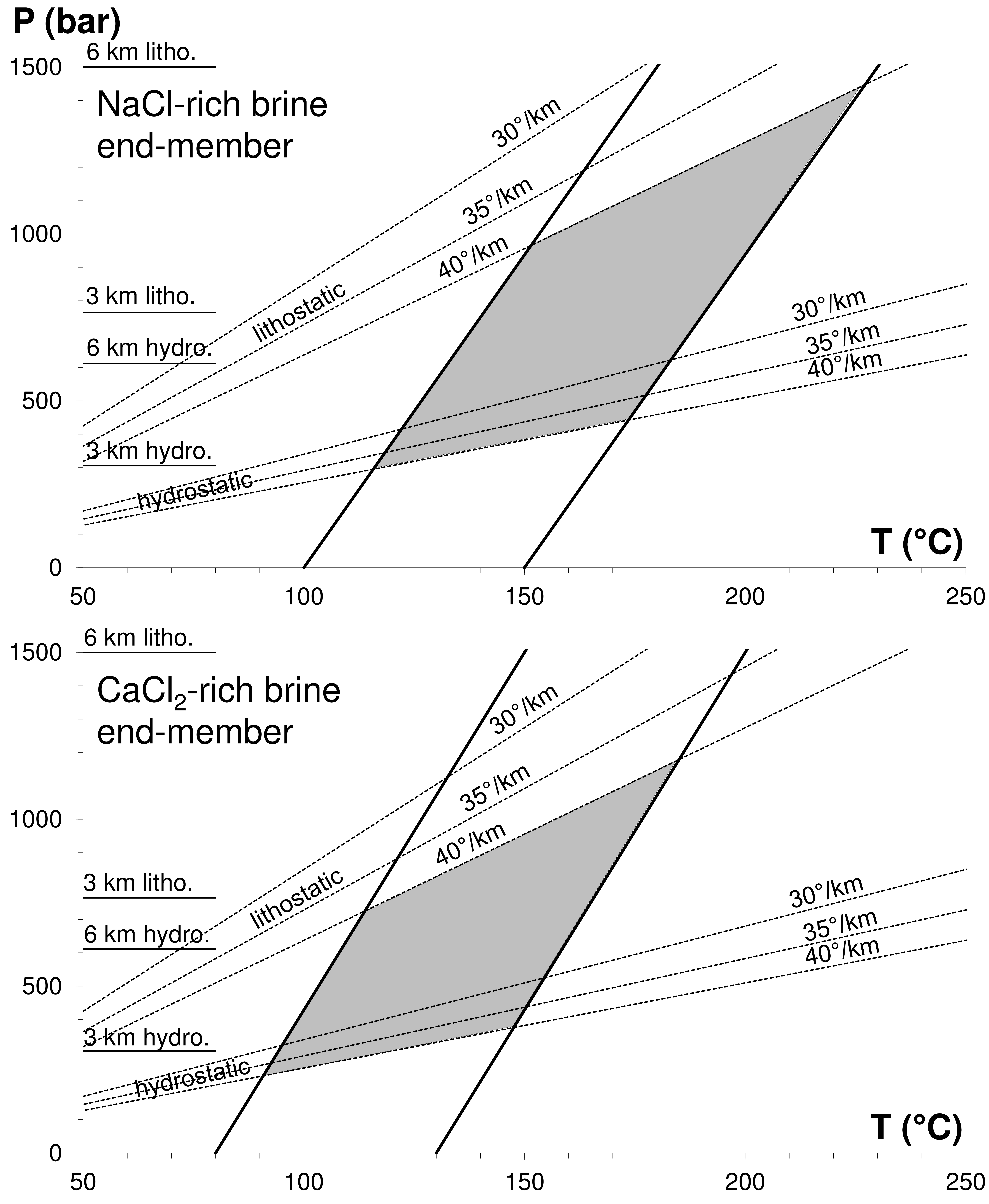
P (bar)
6 km litho.
1500
NaCl-rich brine
end-member
30°/km
35°/km
40°/km
1000
3 km litho.
lithostatic
6 km hydro.
30°/km
35°/km
40°/km
500
3 km hydro.
hydrostatic
T (°C)
0
50
100
150
200
250
6 km litho.
1500
CaCl$_2$-rich brine
end-member
30°/km
35°/km
40°/km
1000
3 km litho.
lithostatic
6 km hydro.
30°/km
35°/km
40°/km
500
3 km hydro.
hydrostatic
T (°C)
0
50
100
150
200
250

FIGURE 9

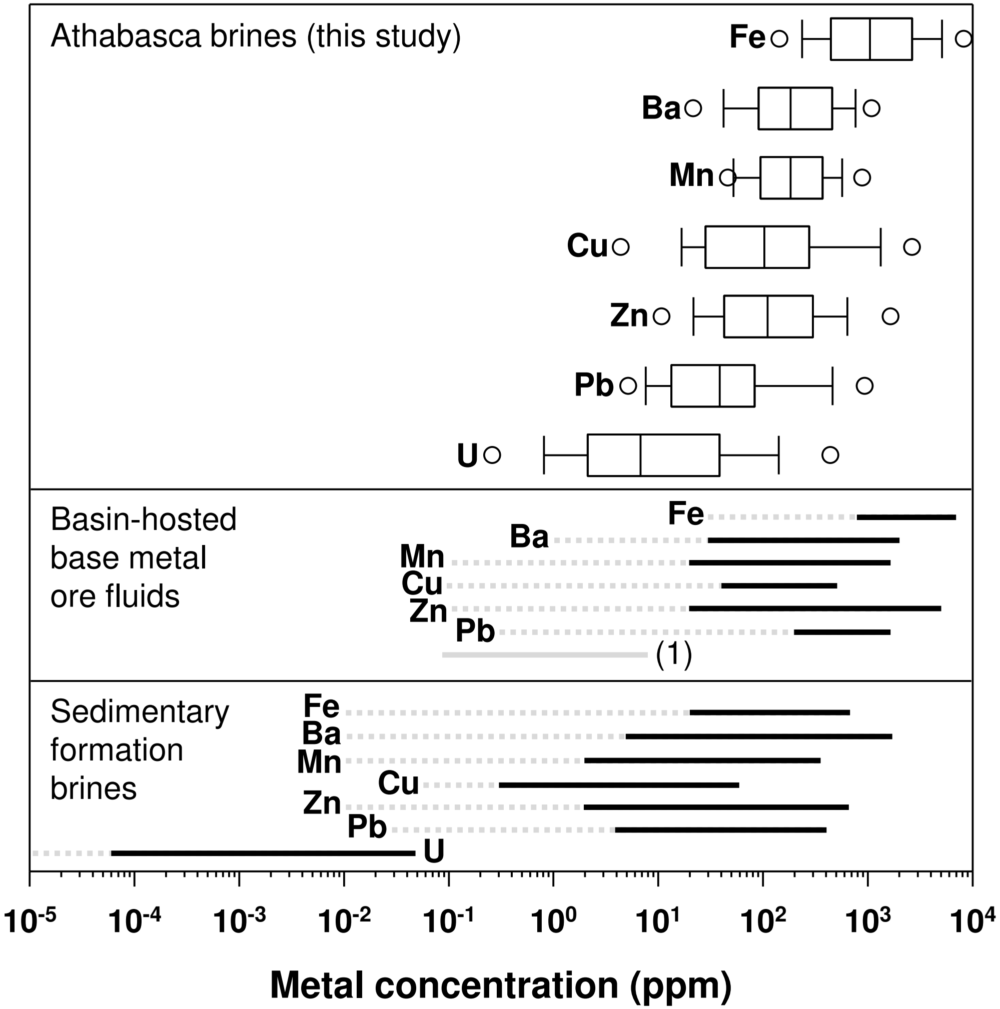
Athabasca brines (this study)
Fe
Ba
Mn
Cu
Zn
Pb
U
Basin-hosted base metal ore fluids
Fe
Ba
Mn
Cu
Zn
Pb
(1)
Sedimentary formation brines
Fe
Ba
Mn
Cu
Zn
Pb
U
10^{-5}
10^{-4}
10^{-3}
10^{-2}
10^{-1}
10^{0}
10^{1}
10^{2}
10^{3}
10^{4}
Metal concentration (ppm)

FIGURE 10

Table 1

	NaCl-rich brine			$CaCl_2$-rich brine	
	End-member compositions from LA-ICP-MS				
Na (ppm)	80000 to 100000			20000 to 40000	
Ca (ppm)	20000 to 50000			80000 to 130000	
Mg (ppm)	2000 to 10000			30000 to 70000	
K (ppm)	1000 to 5000			10000 to 35000	
U (ppm)	100 to 500			1 to 10	
	Microthermometric characteristics				
Fluid inclusion types	Lw1	Lw2	Lwh	Lw'	Lwh'
NaCl at room T°	no	no	yes	no	yes
Last phase to melt	ice	hyd.	hyd.	ice	ice
Te (°C)	-75 to -50	-75 to -50	-75 to -50	-75 to -60	-75 to -60
Tm ice (°C)	-25 to -11.2	-28.8 to -21	-27.7 to -24	-60 to -30	-58 to -36
Tm hyd (°C)	-	-7 to 21.9	-3.2 to 19.2	-	-
Ts NaCl (°C)	-	-	99.5 to 208	-	115 to 235
Th (°C) mode	165	165	135	115	115
	Composition from microthermometry, Raman and LIBS				
	Lw1	Lw2	Lwh	Lw'	Lwh'
Cl (molal)	3 to 4.5	5.5 to 6.5	6.5	6	6.5
Na/Ca (mole)	4.6	3 to 7.7	3.8	0.5	0.8
Ca/Mg (mole)	1	1 to 17.9	-	1.5	1.7
wt.% NaCl	14	22 to 24	25	5	8
wt.% $CaCl_2$	6	6 to 12	13	20	19
wt.% $MgCl_2$	4	0 to 0.9	0	11.5	9.5

Table 2

Locality	Reference	Sample description	Fluid inclusion types				
			NaCl-rich brine			$CaCl_2$-rich brine	
			Lw1	Lw2	Lwh	Lw'	Lwh'
McArthur River	1, 2, 3, 4	Quartz overgrowths in sandstones	yes			yes	yes
		Quartz cementing veins and breccias	yes	yes	yes	yes	yes
P-Patch	5	Magmatic and metamorphic quartz	yes	yes	yes	yes	yes
Rabbit Lake	6	Quartz cementing veins and breccias			yes		yes
		Dolomite cementing veins and breccias		yes	yes		
Shea Creek	7	Magmatic and metamorphic quartz	yes				
Midwest	8	Unknown			yes		
Eagle Point	3	Quartz cementing veins and breccias			yes		yes
Cluff Lake	9, 10	Quartz overgrowths in sandstones	yes		yes	yes	yes
Sue C - McClean	11	Quartz cementing veins and breccias	yes		yes	yes	yes
Rumpel Lake	9, 10, 12	Quartz overgrowths in sandstones	yes		yes	yes	yes
Millennium	13	Quartz cementing veins and breccias	yes				
		Metamorphic quartz	yes				
Key Lake	14	Quartz overgrowths in sandstones			yes		